Stability of multiple-crossarm prestressed stayed columns with additional stay systems

Luke Lapira, M. Ahmer Wadee*, Leroy Gardner

Department of Civil and Environmental Engineering, Imperial College London, South Kensington Campus, London SW7 2AZ, UK

Abstract

Prestressed stayed columns have an enhanced resistance to buckling through the effective use of crossarms and pretensioned stays when compared to conventional columns. An analytical derivation of the minimum, linear optimum and maximum initial pretension forces for configurations of prestressed stayed columns with multiple crossarms and additional stays is presented for the first time. The findings are validated through comparisons with finite element models developed in the commercial package ABAQUS. The influence of the initial pretension on the load-carrying capacity of the configurations considered is also analysed, providing insight into the actual optimum initial pretension force for the configurations accounting for the significance of geometric nonlinearities.

Keywords: Prestressed stayed columns; Steel structures; Analytical modelling; Structural stability; Finite element analysis; Nonlinearity; Cables

1. Introduction

Prestressed stayed columns, the composition of which includes a main column element, a system of crossarm members and pretensioned cable stays, offer an aesthetic, innovative and practical solution to enhancing the buckling strength of slender columns. Their enhanced resistance to buckling arises from the effective provision of intermediate supports through the crossarms and the stay system. The net result is that the column buckling length is reduced thereby increasing the critical buckling load. Although not currently covered by design codes explicitly, prestressed stayed columns are often found in construction owing to their structural efficiency and aesthetic value. Figure 1 shows an example in practice from the development at Chiswick Park in London, whereby a triple-crossarm stayed column with additional stays is used to support a shading structure at roof level.

Prior to the mid 1970s [1], research on prestressed stayed columns focused on cases where a small amount of residual tension in the stays was present prior to buckling. How-

*Corresponding author

Email addresses: luke.lapira15@imperial.ac.uk (Luke Lapira), a.wadee@imperial.ac.uk (M. Ahmer Wadee), leroy.gardner@imperial.ac.uk (Leroy Gardner)

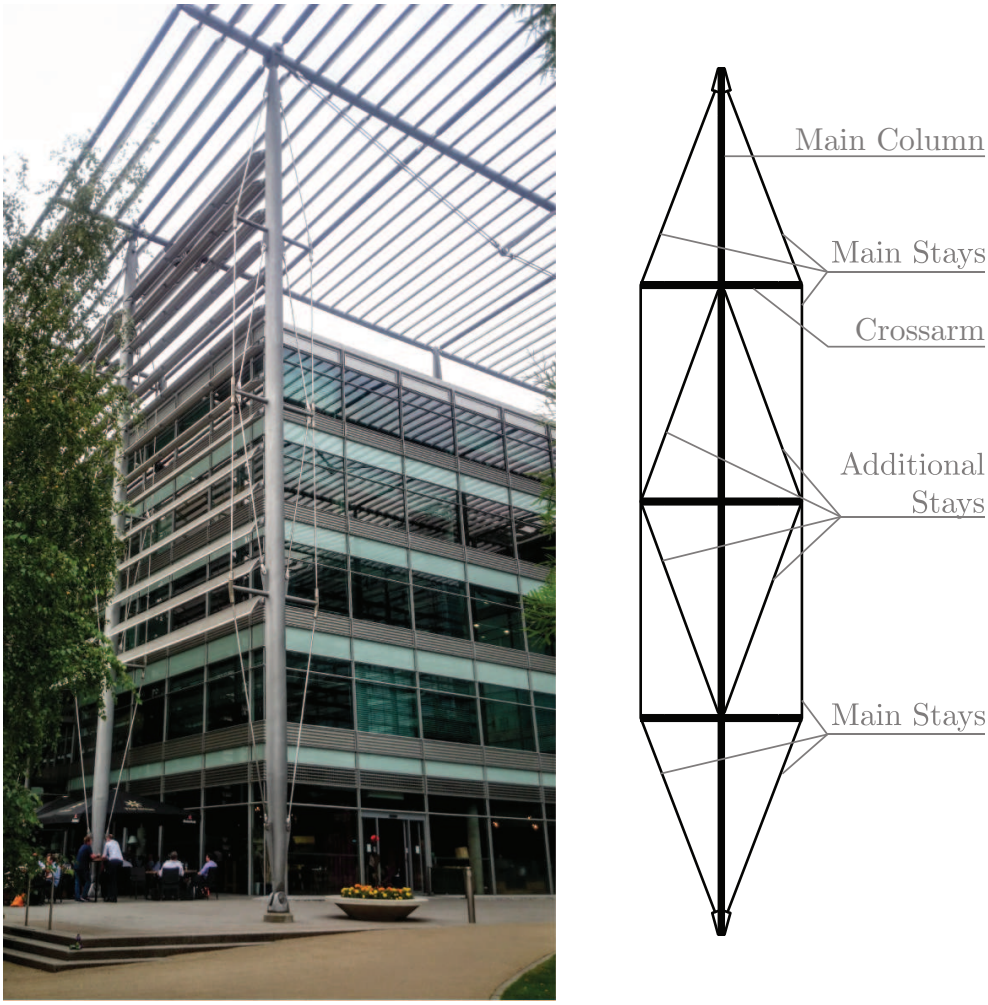

Figure 1: Triple-crossarm stayed column with additional stays at Building 5, Chiswick Park, London, UK.

ever, the detailed effect of different levels of pretension on the mechanical behaviour had not been explored. Subsequently [2], three zones of behaviour were demarcated by the following pretensioning force levels: $T_{\min}$, T_{opt} and $T_{\max}$, as shown in Figure 2 where:

- $T_{\min}$ is the minimum initial pretension force that ensures the buckling load is higher than the classical Euler load P_{E} of the bare, unstayed, main column element. This denotes the transition between Zones 1 and 2 where the pretension force begins to affect the buckling load significantly.

- T_{opt} is the initial pretension force at which all the stays lose their tensile force simultaneously at the maximum possible buckling load, denoted as $P_{\max}$. This denotes the transition between Zones 2 and 3 where, in the latter, there is a residual tension in the stays when buckling is triggered.

- $T_{\max}$ is the pretension force that causes buckling without the application of any

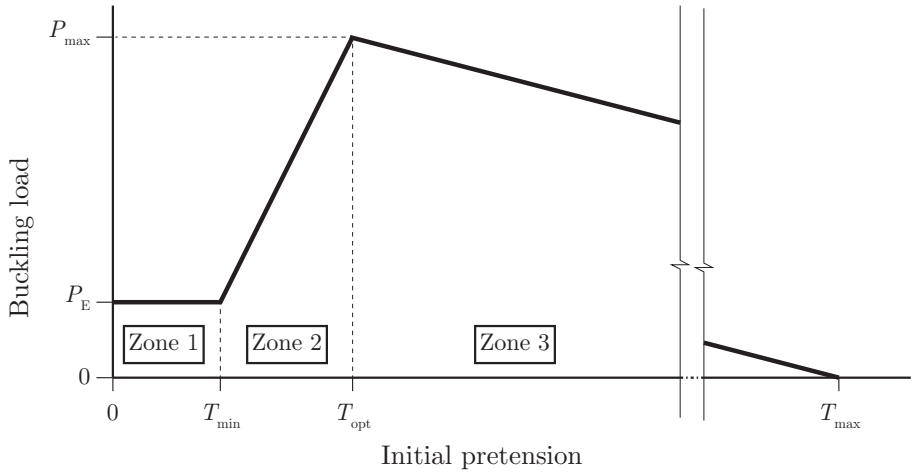

Figure 2: Critical buckling load versus initial pretension force T, as determined in [2].

external load.

However, from later studies [3, 4, 5, 6, 7] it was determined that the zonal behaviour is only part of the story. Although, the identified zones provide important insight into the behaviour as a function of the initial pretension, in reality the ultimate load is greater than the Euler load at low pretensioning levels and rises with increasing pretension beyond T_{opt}, before reaching a peak and finally reducing with increasing T. It was shown in [6] and [7] that T_{opt} is significantly below the initial pretension force that truly maximizes the load-carrying capacity when large deflections are considered. This effect is primarily due to the nonlinear post-buckling behaviour where bending of the main column reactivates stays that had gone slack during the triggering of critical buckling [8]. However, since T_{opt} demarcates between distinct linear buckling behaviours, it is considered to be the benchmark initial pretension in the current work; it is henceforth termed the 'linear optimal' initial pretension force to distinguish it from the true optimal value.

A significant volume of research has been carried out on prestressed stayed columns where the theory underpinning the ultimate resistance has been investigated [4, 9, 6, 10], the post-buckling behaviour has been established [8, 11, 12, 13], interactive buckling has been studied [14, 15] and experiments have been conducted [16, 17, 18]. As far as the authors are aware, there is very little published research that considers the behaviour of multiple crossarm stayed columns with additional stays. Temple [19] considered multiple crossarm configurations including additional stays to determine the adequacy of the finite element (FE) method for predicting the linear buckling loads. Van Steirteghem *et al* [20] analysed stayed columns with bipod configurations, determining that a significant increase in efficiency may be achieved by using a split crossarm, as opposed to the single crossarm. More recently, Martins *et al* [21] presented findings from full-scale experiments conducted on 18 metre long double-crossarm configurations.

The current work focuses on the effects on having additional stays on the behaviour of prestressed stayed columns with multiple crossarms along the length. The derivations

of the linear optimal prestress, as determined in [2] for single-crossarm stayed columns, are extended to such configurations first. A parametric FE study to validate the key prestress levels obtained is then presented. Finally, the behaviour of the configurations under different degrees of initial pretension is explored and conclusions are then drawn.

2. Analytical modelling

The restraint introduced by the stays in prestressed stayed columns at the location of the crossarms is dependent on the initial geometry and the level of the initial pretension within the stays. Figure 3 shows a sequence of increasingly sophisticated configurations of

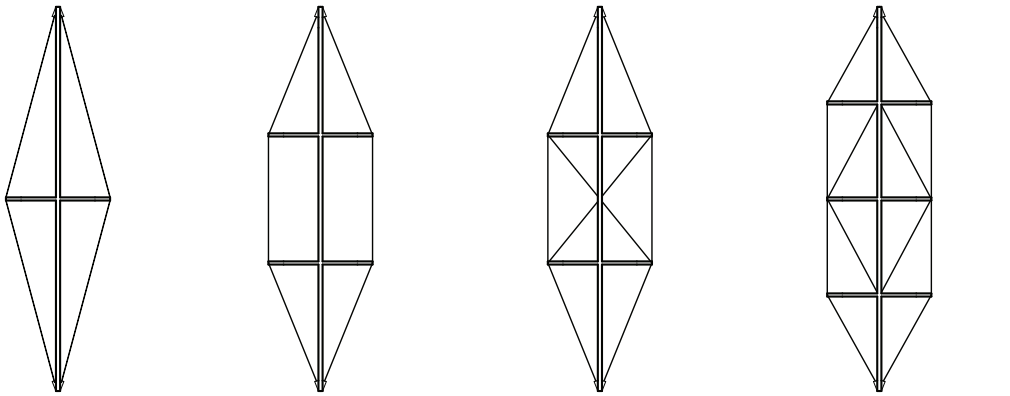

Figure 3: Configurations of the considered prestressed stayed columns.

prestressed stayed columns from a single and a double crossarm stayed column with only one stay-group (Configuration 1) to a double and triple crossarm case with two stay-groups (Configurations 2 and 3 respectively). Upon application of the external load, the elastic pre-buckling deformations result in the shortening of the stays causing a reduction in the lateral restraint provided. The influence of the additional stay-group on the behaviour of the stayed column is therefore determined by considering such deformations. The discussion first examines the more complex deformation relationships of Configuration 3 and then for Configuration 2 since the former introduces the majority of terms and relationships. The improvements in load-carrying capacity for these configurations with two stay-groups are then compared to the results from the reference case of Configuration 1, which contains only one stay-group.

2.1. Assumptions

As in the work presented in [2], the following assumptions are made in deriving the key prestress levels for the configurations considered.

1. The member has reflective symmetry and is axially loaded with no initial imperfections.

2. The crossarm to column connections are rigid, while the connections between the stays and the crossarm and between the stays and the main column are pinned.
3. Axial deformations of the column and crossarm members influence the force in the stays with no implications on the maximum buckling load for the member, *i.e.* any slight increase (or decrease) in the buckling loads of the main column element or the crossarms from shortening (or lengthening) is neglected.
4. Elastic analyses are conducted and only small angle changes are assumed throughout.
5. Initial pretensioning forces within the stays are limited based on the relationships established by means of free-body diagrams. This ensures that the crossarms remain straight and perpendicular to the column upon application of the external load.

As is the case in the derivations of similar expressions for single crossarm configurations, the assumptions presented above highlight the range of applicability and hence limitations of the derived expressions. In particular, the validity of the expressions presented is limited to linear elastic material behaviour and to the range where the pre-buckling deformations presented in Figures 4(a) and 7(a) remain small. Since the global slenderness of the main column element tends to be relatively high in prestressed stayed columns, these assumptions are not particularly restrictive for practical geometries.

2.2. Geometric analysis of pre-buckling deformations in Configuration 3

Consider an ideal pin-ended triple-crossarm stayed column with additional stays and pre-buckling deformations, as depicted in Figure 4(a). Member forces P, F and T represent the internal forces in the column, crossarms and stays respectively. It is assumed that the angles α, β and γ do not change significantly as the pretension forces within the cables are introduced, hence $\alpha_1 \approx \alpha$, $\beta_1 \approx \beta$ and $\gamma \approx 0$. For the free-body diagrams shown in Figure 4(b), the internal member forces initially (*i.e.* after prestressing) and after the application of the external load P are:

$$P_i = 2T_{1,i}\cos\alpha + 2T_{2,i}\cos\beta, \tag{1}$$

$$F_{1,i} = T_{1,i}\sin\alpha, \quad F_{2,i} = 2T_{2,i}\sin\beta, \tag{2}$$

$$P_f = P + 2T_{1,f}\cos\alpha + 2T_{2,f}\cos\beta, \tag{3}$$

$$F_{1,f} = T_{1,f}\sin\alpha, \quad F_{2,f} = 2T_{2,f}\sin\beta, \quad T_{3,i} = T_{1,i}\cos\alpha, \tag{4}$$

where P_i, $F_{1,i}$ and $F_{2,i}$ are the initial internal forces in the respective members with P_f, $F_{1,f}$ and $F_{2,f}$ being the internal forces after the application of the external load.

The restraint provided to the column at the location of the crossarms is most effective when the net horizontal force provided by the crossarm is perpendicular to the column and the crossarm is acting axially. While the initial pretension in each of the three groups of stays may be specified independently, Equation (4) represents the condition for the final assumption, thus ensuring the pre-buckling deformed shape is consistent with that in Figure 4(a). Consequently, $T_{3,i}$ is no longer an independent variable in the behaviour.

Having derived the internal forces in the stayed column initially and after the application of the external load (but prior to buckling), the change in length of each element can

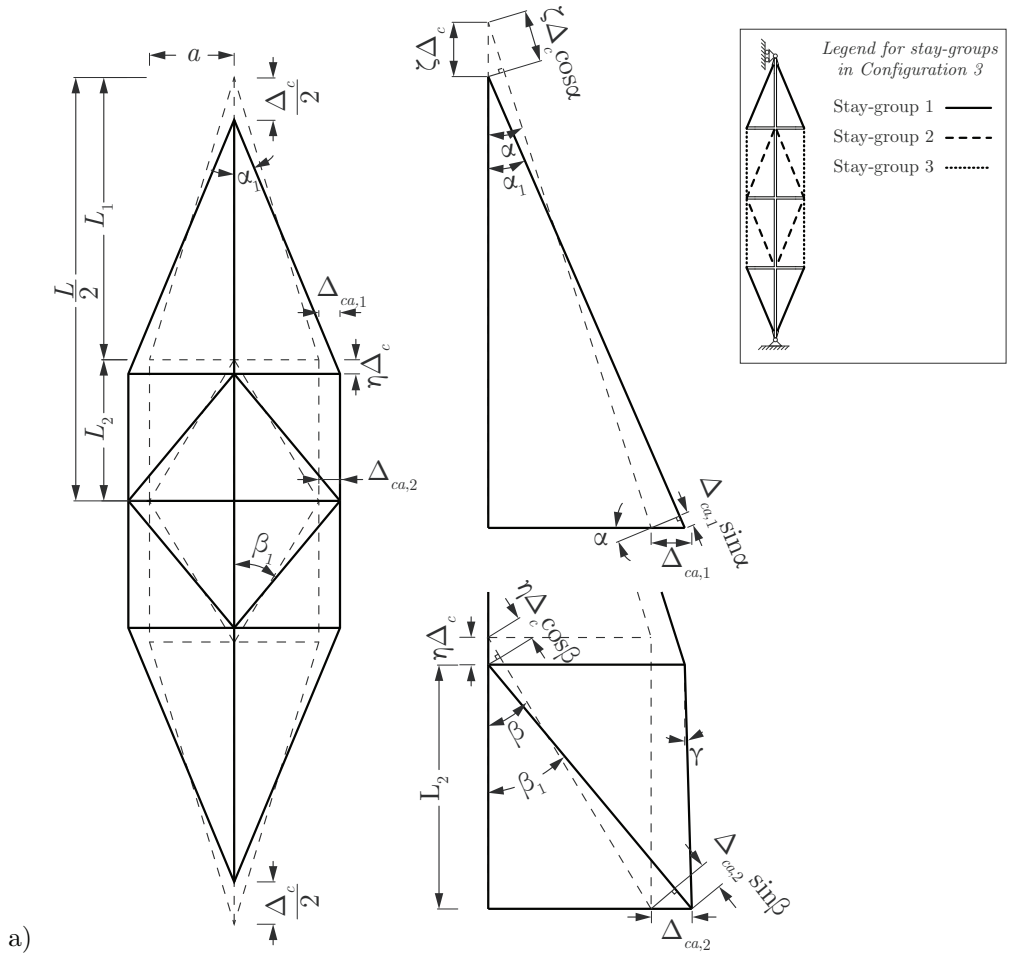

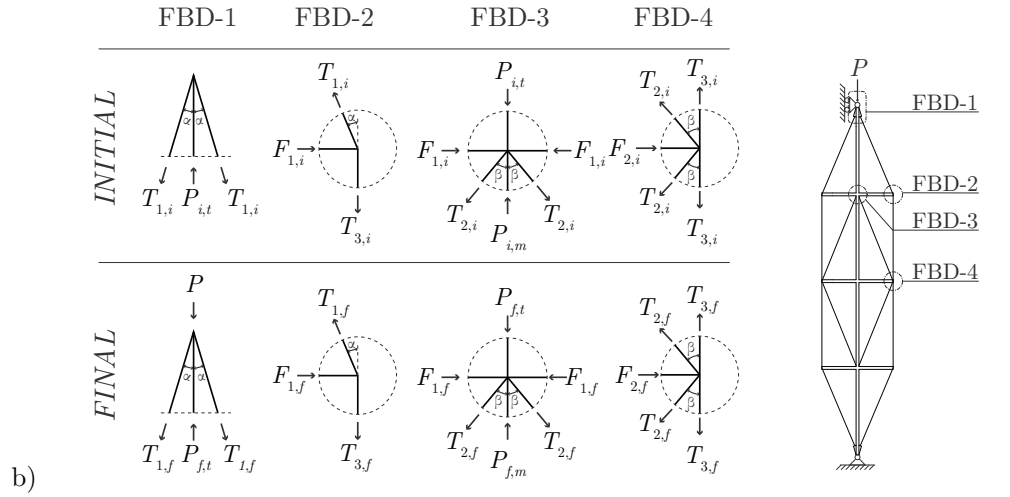

Figure 4: (a) Pre-buckling deformations and geometrical relationships for Configuration 3. (b) Free-body diagrams of forces in members initially and after application of the external load.

be obtained. The expressions for the shortening of stay n, $\Delta_{s,n}$ are found to be:

$$\Delta_{s,1} = \zeta\Delta_c \cos\alpha - \Delta_{ca,1} \sin\alpha, \tag{5}$$
$$\Delta_{s,2} = \eta\Delta_c \cos\beta - \Delta_{ca,2} \sin\beta, \tag{6}$$
$$\Delta_{s,3} = \eta\Delta_c, \tag{7}$$

where:

$$\zeta = \frac{\omega}{2(1+\omega)}, \quad \eta = \frac{1}{2(1+\omega)}, \quad \omega = \frac{\cos\alpha}{\cos\beta}. \tag{8}$$

Equations (5)–(7) highlight the relationship between the shortening of the stays, the shortening of the column and the lengthening of the crossarms. The shortening of the column Δ_c is defined thus:

$$\Delta_c = \frac{P_f - P_i}{K_c}, \tag{9}$$

where K_c is the stiffness of the main column member, defined as:

$$K_c = \frac{E_c A_c}{L}, \tag{10}$$

where E_c is the Young's modulus, A_c is the cross-sectional area and L is the length of the main column element. Substituting the expressions for P_i and P_f into Equation (9) gives:

$$\Delta_c = \frac{P - 2\left[\cos\alpha(T_{1,i} - T_{1,f}) + \cos\beta(T_{2,i} - T_{2,f})\right]}{K_c}. \tag{11}$$

The application of an external load causes a reduction in the column length, resulting in a reduction of the tensile force within the stays. This reduces the axial force in the crossarms that subsequently lengthens the crossarms, Δ_{ca}. This is defined as:

$$\Delta_{ca,1} = \frac{F_{1,i} - F_{1,f}}{K_{a1}}, \quad \Delta_{ca,2} = \frac{F_{2,i} - F_{2,f}}{K_{a2}}, \tag{12}$$

where $\Delta_{ca,1}$ and $\Delta_{ca,2}$ are the lengthening of the outer and middle crossarms respectively and K_{a1} and K_{a2} are the stiffnesses of the outer and middle crossarms respectively:

$$K_{a1} = \frac{E_a A_{a1}}{a_1}, \quad K_{a2} = \frac{E_a A_{a2}}{a_2}, \tag{13}$$

where E_a is the Young's modulus, A_{an} are the cross-sectional areas and a_n are the lengths of the individual crossarm elements. Substituting the expressions for $F_{1,i}$, $F_{1,f}$, $F_{2,i}$ and $F_{2,f}$ respectively into the expressions in Equation (12) give:

$$\Delta_{ca,1} = \frac{\sin\alpha}{K_{a1}}(T_{1,i} - T_{1,f}), \quad \Delta_{ca,2} = \frac{2\sin\beta}{K_{a2}}(T_{2,i} - T_{2,f}). \tag{14}$$

Similarly, the shortening of the stays is defined as:

$$\Delta_{s,1} = \frac{T_{1,i} - T_{1,f}}{K_{s1}}, \quad \Delta_{s,2} = \frac{T_{2,i} - T_{2,f}}{K_{s2}}, \quad \Delta_{s,3} = \frac{T_{3,i} - T_{3,f}}{K_{s3}}, \tag{15}$$

where K_{s1}, K_{s2} and K_{s3} are the stiffnesses of the three stay-groups respectively that are defined thus:

$$K_{s1} = \frac{E_s A_s}{L_{s1}}, \quad K_{s2} = \frac{E_s A_s}{L_{s2}}, \quad K_{s3} = \frac{E_s A_s}{L_{s3}}, \tag{16}$$

where E_s is the Young's modulus, A_s is the cross-sectional area and L_{sn} are the lengths of the stay elements. For stay-group 1, substituting the expressions for Δ_c, $\Delta_{ca,1}$ and $\Delta_{s,1}$ into Equation (5) and rearranging gives:

$$(T_{1,i} - T_{1,f}) = C_{31} \left[P - 2\cos\beta (T_{2,i} - T_{2,f}) \right], \tag{17}$$

where:

$$C_{31} = \frac{\zeta \cos\alpha}{K_c \left(\frac{1}{K_{s1}} + \frac{2\zeta \cos^2\alpha}{K_c} + \frac{\sin^2\alpha}{K_{a1}} \right)}. \tag{18}$$

Similarly, for stay-group 2, substituting the expressions for Δ_c, $\Delta_{ca,2}$ and $\Delta_{s,2}$ into Equation (6) and rearranging gives:

$$(T_{2,i} - T_{2,f}) = C_{32} [P - 2\cos\alpha (T_{1,i} - T_{1,f})], \tag{19}$$

where:

$$C_{32} = \frac{\eta \cos\beta}{K_c \left(\frac{1}{K_{s2}} + \frac{2\eta \cos^2\beta}{K_c} + \frac{2\sin^2\beta}{K_{a2}} \right)}. \tag{20}$$

The application of small angle assumptions implies that $\cos\alpha$ and $\cos\beta$ are basically invariant during loading and therefore Equations (17) and (19) indicate linear relationships between the applied load and the force in the stays. As in [2], the shortening of the column can be defined in terms of the final load in the column and the applied initial pretension force by substituting the expression for P into Equation (9), which gives:

$$\Delta_c = \frac{P_f - 2\left(T_{1,i}\cos\alpha + T_{2,i}\cos\beta\right)}{K_c}. \tag{21}$$

Substituting Δ_c, $\Delta_{ca,1}$ and $\Delta_{s,1}$ into Equation (5) and rearranging gives the final tension in stay-group 1, thus:

$$T_{1,f} = T_{1,i} - C_{33} \left[P_f - 2\left(T_{1,i}\cos\alpha + T_{2,i}\cos\beta\right) \right], \tag{22}$$

where:

$$C_{33} = \frac{\zeta \cos\alpha}{K_c \left(\frac{1}{K_{s1}} + \frac{\sin^2\alpha}{K_{a1}} \right)}. \tag{23}$$

Similarly, substituting Δ_c, $\Delta_{ca,2}$ and $\Delta_{s,2}$ into Equation (6) and rearranging gives the final tension in stay-group 2, thus:

$$T_{2,f} = T_{2,i} - C_{34} \left[P_f - 2\left(T_{1,i}\cos\alpha + T_{2,i}\cos\beta\right) \right], \tag{24}$$

where:

$$C_{34} = \frac{\eta \cos\beta}{K_c \left(\frac{1}{K_{s2}} + \frac{2\sin^2\beta}{K_{a2}} \right)}. \tag{25}$$

Finally, substituting for $T_{1,f}$ and $T_{2,f}$ into Equation (3) and rearranging leads to:

$$P = C_{35} \left[P_f - 2 \left(T_{1,i} \cos\alpha + T_{2,i} \cos\beta \right) \right], \tag{26}$$

where:

$$C_{35} = 1 + 2 \left(C_{33} \cos\alpha + C_{34} \cos\beta \right), \tag{27}$$

and this results in the externally applied load being expressed in terms of the initial tension in the stays and the final axial load within the column. Equation (27) shows another linear relationship between these parameters.

2.3. Determination of the zonal boundaries for Configuration 3

In Zones 1 and 2, as deduced in [2], the buckling load is defined at the instant where the force in any of the stays vanishes. The same definitions are used currently to obtain similar relationships. Owing to the presence of multiple stay-groups, the zones are dependent on the interaction of the initial pretension forces, T_1 and T_2, being the independent variables in the structural system. By definition, in Zones 1 and 2, $T_{1,f} = T_{2,f} = 0$ and the transitions between Zones 1–2 and 2–3 are defined by an interaction between $T_{1,i}$ and $T_{2,i}$, as shown in Figure 5.

The minimum effective initial pretension $T_{1,\min}$ and $T_{2,\min}$ are derived by setting P equal to the classical Euler load of the main column element $P_{\mathrm{E}} = \pi^2 E_c I_c / L^2$, where I_c is the second moment of area of the main column element about the axis of buckling, in Equations (17) and (19). The solutions are summarized thus:

$$T_{1,\min} = C_{31} \left(P_{\mathrm{E}} - 2T_{2,i} \cos\beta \right), \quad T_{2,\min} = C_{32} \left(P_{\mathrm{E}} - 2T_{1,i} \cos\alpha \right) \tag{28}$$

$$T_{1,\min,0} = C_{31} P_{\mathrm{E}}, \quad T_{2,\min,0} = C_{32} P_{\mathrm{E}}, \tag{29}$$

where $T_{1,\min,0}$ is the minimum initial pretension required in stay-group 1 when $T_{2,i} = 0$, and vice-versa for $T_{2,\min,0}$. The expressions in Equation (28) define the boundary between Zones 1 and 2. Solving for $T_{1,i}$ and $T_{2,i}$ simultaneously from Equations (17) and (19) result in the following expressions:

$$T_{1,\min,2} = \frac{C_{31} P_{\mathrm{E}} (1 - 2C_{32} \cos\beta)}{1 - 4C_{31} C_{32} \cos\alpha \cos\beta}, \quad T_{2,\min,1} = \frac{C_{32} P_{\mathrm{E}} (1 - 2C_{31} \cos\alpha)}{1 - 4C_{31} C_{32} \cos\alpha \cos\beta}, \tag{30}$$

where $T_{1,\min,2}$ is the value obtained for $T_{1,i}$ in terms of $T_{2,i}$ and vice-versa for $T_{2,\min,1}$. The point $(T_{1,\min,2}, T_{2,\min,1})$ on the T_1T_2 plane gives the transition point between the equations shown in Figure 5(a).

A similar relationship between $T_{1,i}$ and $T_{2,i}$ for the transition between Zones 2–3 is derived using the same methodology with $P = P_{\max}$. A linear buckling analysis is used to determine the theoretical maximum load-carrying capacity of the prestressed stayed

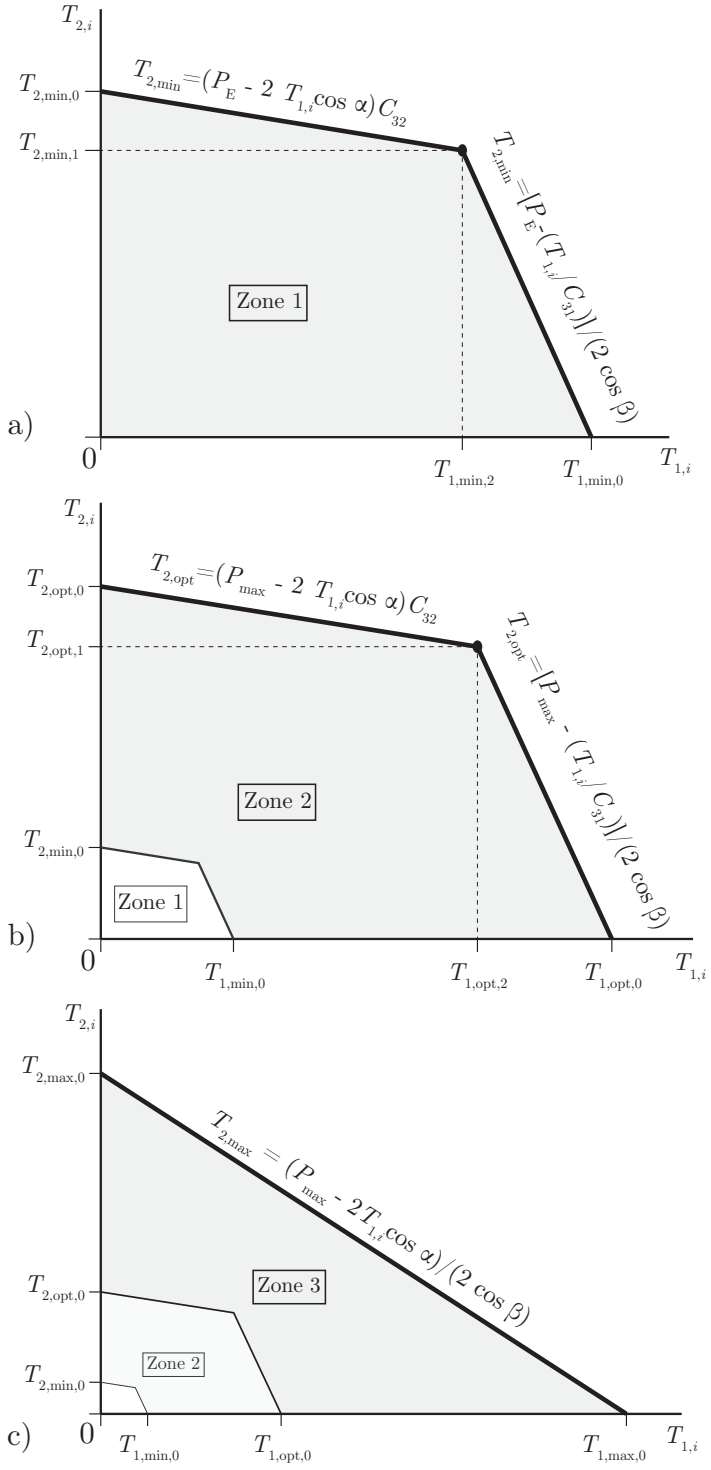

Figure 5: Initial pretensioning force interaction relationships for Configuration 3; $T_{2,i}$ versus $T_{1,i}$ for responses within: (a) Zone 1 and (b) Zone 2. (c) Theoretical limits of $T_{1,i}$ and $T_{2,i}$.

column configuration in the presence of the stays and no pretension applied, $P_{\mathrm{T}=0}$. This methodology has been confirmed to be acceptable in [2, 6]; $P_{\max}$ is obtained by substituting $T_{1,i} = T_{2,i} = 0$ into Equation (26), giving:

$$P_{\max} = \frac{P_{T=0}}{C_{35}}, \tag{31}$$

$$T_{1,\mathrm{opt}} = C_{31}\left(P_{\max} - 2T_{2,i}\cos\beta\right), \quad T_{2,\mathrm{opt}} = C_{32}\left(P_{\max} - 2T_{1,i}\cos\alpha\right) \tag{32}$$

$$T_{1,\mathrm{opt},0} = C_{31}P_{\max}, \quad T_{2,\mathrm{opt},0} = C_{32}P_{\max}, \tag{33}$$

$$T_{1,\mathrm{opt},2} = \frac{P_{\max}C_{31}(1 - 2C_{32}\cos\beta)}{1 - 4C_{31}C_{32}\cos\alpha\cos\beta}, \quad T_{2,\mathrm{opt},1} = \frac{P_{\max}C_{32}(1 - 2C_{31}\cos\alpha)}{1 - 4C_{31}C_{32}\cos\alpha\cos\beta}, \tag{34}$$

and Figure 5(b) illustrates the results from the relationships in Equations (32)–(34).

The theoretical maximum initial pretension is that which causes the stayed column to buckle without the application of any external load. Substituting for $P = 0$ into Equation (26) while including the fact that $P_f = P_{\max}$, yields the following relationship:

$$P_{\max} = 2\left(T_{1,\max}\cos\alpha + T_{2,\max}\cos\beta\right), \tag{35}$$

and Figure 5(c) illustrates this relationship between $T_{1,\max}$ and $T_{2,\max}$.

2.4. Theoretical buckling load for Zones 1–3 in Configuration 3

For a particular geometry, Figure 6 depicts the relationship between the buckling load obtained from the equations presented and the initial pretension. The following procedure is proposed to determine the buckling load analytically.

1. Calculate: $T_{1,\min,0}$, $T_{1,\min,2}$, $T_{1,\mathrm{opt},0}$, $T_{1,\mathrm{opt},2}$, $T_{1,\max,0}$, $T_{2,\min,0}$, $T_{2,\min,1}$, $T_{2,\mathrm{opt},0}$, $T_{2,\mathrm{opt},1}$, $T_{2,\max,0}$.
2. Establish a value for $T_{2,i}$, hence if:
   - $T_{2,i} \leqslant T_{2,\min,1}$, solve for $T_{1,\min}$ and $T_{1,\mathrm{opt}}$ using Equation (17);
   - $T_{2,\min,1} < T_{2,i} < T_{2,\min,0}$, solve for $T_{1,\min}$ using Equation (19) and $T_{1,\mathrm{opt}}$ using Equation (17);
   - $T_{2,i} < T_{2,\mathrm{opt},1}$, $T_{1,\min} = 0$ and $T_{1,\mathrm{opt}}$ is solved for using Equation (17);
   - $T_{2,\mathrm{opt},1} < T_{2,i} < T_{2,\min,0}$, $T_{1,\min} = 0$ and $T_{1,\mathrm{opt}}$ is solved for using Equation (19);
   - $T_{2,i} > T_{2,\mathrm{opt},0}$, the column is in Zone 3 and $T_{1,\min} = T_{1,\mathrm{opt}} = 0$.
3. Having established $T_{2,i}$ and the limits for Zones 1–3, the critical buckling load P^{C} is determined based on the value of $T_{1,\mathrm{i}}$ selected, where:
   - Zone 1: $P^{\mathrm{C}} = P_{\mathrm{E}}$;
   - Zone 2: P^{C} is the maximum of P evaluated from Equations (17) and (19);
   - Zone 2–3 boundary: $P^{\mathrm{C}} = P_{\max}$;
   - Zone 3: P^{C} is derived from Equation (26).

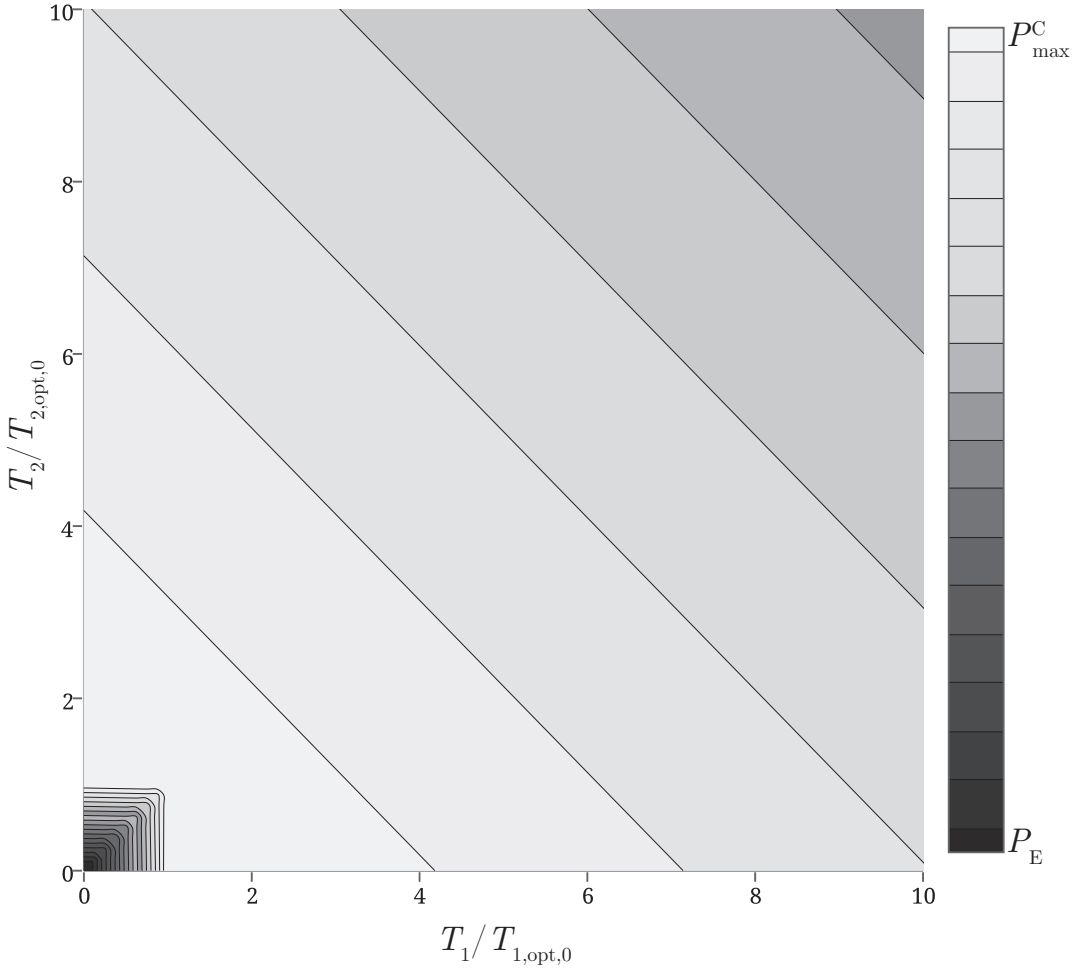

Figure 6: Contour plot of the critical buckling load P^{C} plotted against the initial pretension forces $T_{1,i}$ and $T_{2,i}$, depicted for $\omega = 1$, which represents the stayed column configuration where the angles $\alpha = \beta$.

2.5. Determination of the zonal boundaries for Configuration 2

In Configuration 2, for the assumed pre-buckling deformation shown in Figure 7, the following relationship can be determined:

$$T_{3,i} = T_{1,i}\cos\alpha - T_{2,i}\cos\beta, \tag{36}$$

thus, $T_{3,i}$ is once again dependent on $T_{1,i}$ and $T_{2,i}$, which are the independent variables. The transitions between Zones 1–2 and 2–3 are also defined by an interaction between $T_{1,i}$ and $T_{2,i}$, as shown in Figure 8. The derivation procedure is similar to that presented in Section 2.2; however for the condition stipulated in assumption 5 in Section 2.1, there are two scenarios to be considered depending on whichever of $T_{1,i}\cos\alpha$ or $T_{2,i}\cos\beta$ is larger.

2.5.1. Case: $T_{1,i}\cos\alpha > T_{2,i}\cos\beta$

The minimum, linear optimal and maximum initial pretensioning forces in Configuration 2 are:

$$T_{1,\min} = C_{21}P_{\mathrm{E}} - C_{21b}T_{2,i}, \quad T_{2,\min} = C_{22}P_{\mathrm{E}} - C_{22b}T_{1,i}, \tag{37}$$

$$T_{1,\min,2} = P_{\mathrm{E}}\left(\frac{C_{21} - C_{21b}C_{22}}{1 - C_{21b}C_{22b}}\right), \quad T_{2,\min,1} = P_{\mathrm{E}}\left(\frac{C_{22} - C_{21}C_{22b}}{1 - C_{21b}C_{22b}}\right), \tag{38}$$

$$T_{1,\mathrm{opt}} = C_{21}P_{\max} - C_{21b}T_{2,i}, \quad T_{2,\mathrm{opt}} = C_{22}P_{\max} - C_{22b}T_{1,i}, \tag{39}$$

$$T_{1,\mathrm{opt},2} = P_{\max}\left(\frac{C_{21} - C_{21b}C_{22}}{1 - C_{21b}C_{22b}}\right), \quad T_{2,\mathrm{opt},1} = P_{\max}\left(\frac{C_{22} - C_{21}C_{22b}}{1 - C_{21b}C_{22b}}\right), \tag{40}$$

$$P_{\max} = 2T_{1,\max}\cos\alpha + \frac{C_{23b}T_{2,\max}}{C_{23}}, \tag{41}$$

where:

$$P_{\max} = \frac{P_{T=0}}{C_{23}}, \tag{42}$$

$$C_{21} = \frac{\zeta\cos\alpha}{K_c\left(\frac{1}{K_{s1}} + \frac{2\zeta\cos^2\alpha}{K_c} + \frac{\sin^2\alpha}{K_{a1}}\right)}, \quad C_{21b} = \frac{\sin\alpha\sin\beta}{\left(\frac{1}{K_{s1}} + \frac{2\zeta\cos^2\alpha}{K_c} + \frac{\sin^2\alpha}{K_{a1}}\right)}, \tag{43}$$

$$C_{22} = \frac{\eta\cos\beta}{K_c\left(\frac{1}{K_{s2}} + \frac{\sin^2\beta}{K_{a1}}\right)}, \quad C_{22b} = \frac{2K_{a1}\eta\cos\alpha\cos\beta + K_c\sin\alpha\sin\beta}{K_{a1}K_c\left(\frac{1}{K_{s2}} + \frac{\sin^2\beta}{K_{a1}}\right)}, \tag{44}$$

$$C_{23} = 1 + \left[\frac{2\zeta\cos^2\alpha}{K_c\left(\frac{1}{K_{s1}} + \frac{\sin^2\alpha}{K_{a1}}\right)}\right], \quad C_{23b} = \frac{\sin 2\alpha\sin\beta}{K_{a1}\left(\frac{1}{K_{s1}} + \frac{\sin^2\alpha}{K_{a1}}\right)}. \tag{45}$$

2.5.2. Case: $T_{2,i}\cos\beta > T_{1,i}\cos\alpha$

In this case, for the pre-buckling deformation in Figure 7(a) to hold true, the relationship between the stay forces is thus:

$$T_1 = \frac{T_2}{\omega}, \tag{46}$$

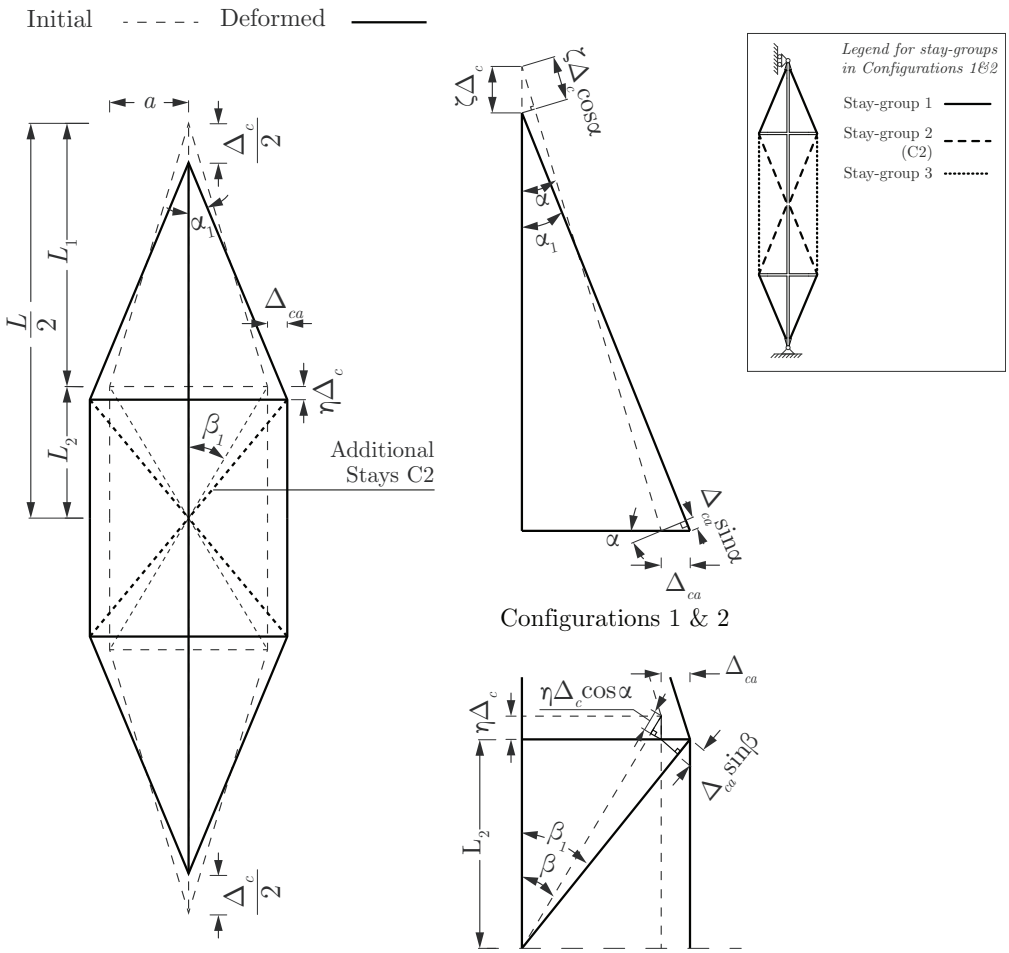

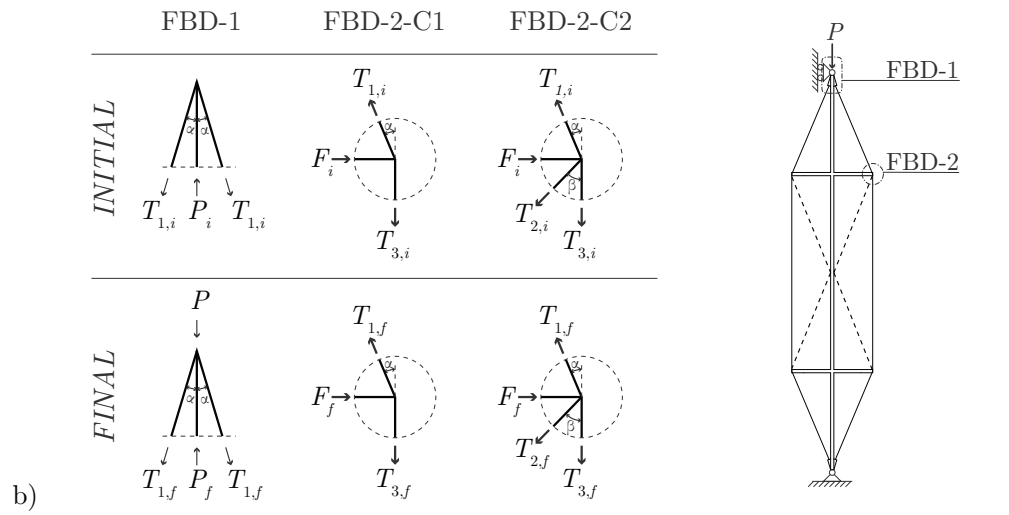

Figure 7: (a) Pre-buckling deformations and geometrical relationships in Configurations 1 and 2. (b) Free-body diagrams of forces in members initially and after the application of the external load.

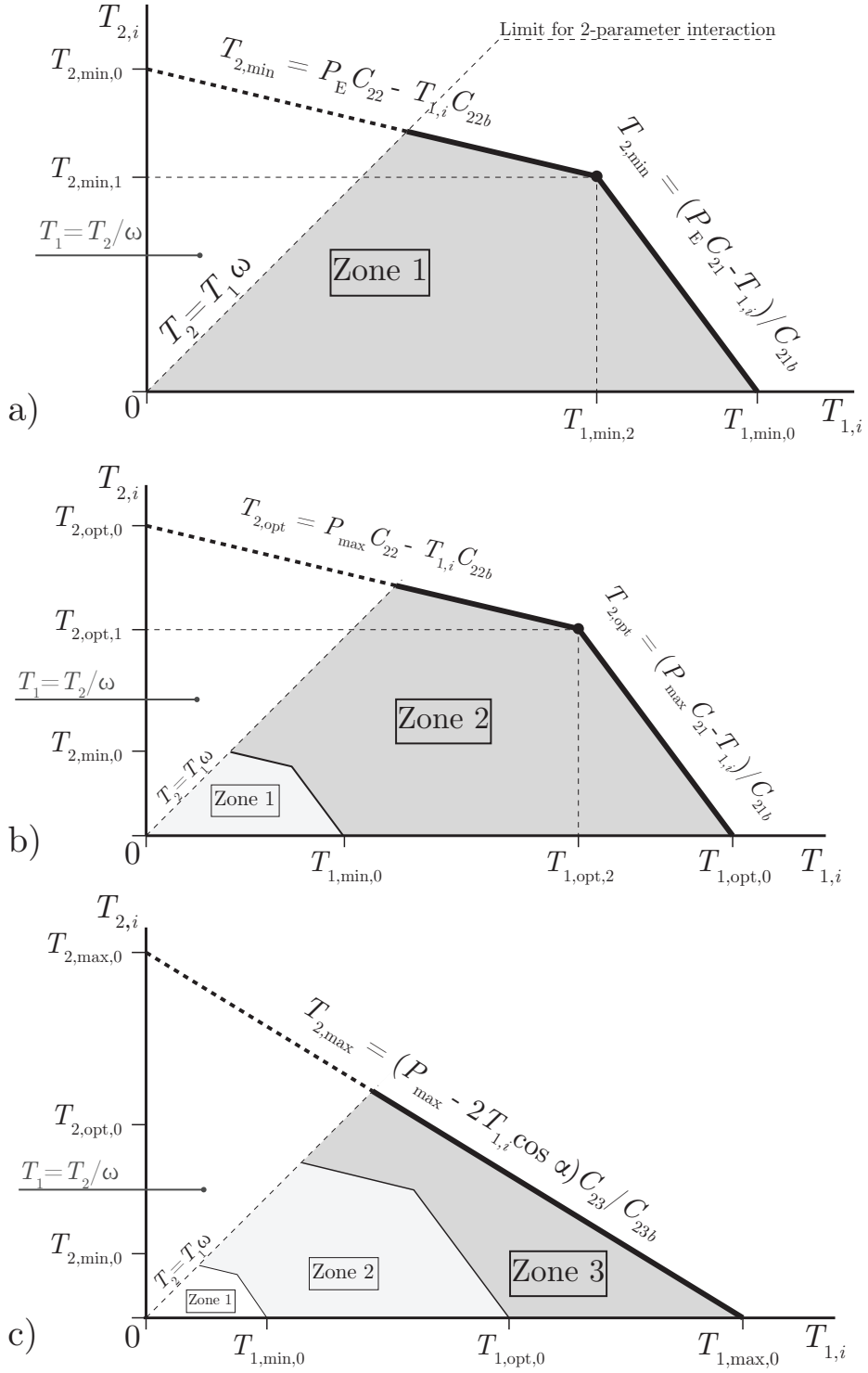

Figure 8: Initial pretensioning force interaction relationships for Configuration 2; $T_{1,i}$ versus $T_{2,i}$ for responses within: (a) Zone 1 and (b) Zone 2. (c) Theoretical limits of $T_{1,i}$ and $T_{2,i}$.

where ω was defined in Equation (8). Hence, $T_{1,i}$ is also a dependent variable, leaving $T_{2,i}$ as the only independent variable. Given this condition and using the same relationships for Zones 1 and 2 as described, the minimum, linear optimal and maximum initial pretensioning forces are thus:

$$T_{2,\min,2} = \min \begin{cases} C_{24a} P_{\mathrm{E}} \\ C_{24b} P_{\mathrm{E}} \end{cases} \tag{47}$$

$$T_{2,\mathrm{opt},2} = \min \begin{cases} C_{24a} P_{\max,2} \\ C_{24b} P_{\max,2} \end{cases} \tag{48}$$

$$P_{\max,2} = \min \begin{cases} P_{T=0}/C_{24a} \\ P_{T=0}/C_{24b} \end{cases} \tag{49}$$

$$T_{2,\max,2} = \frac{P_{\max,2}}{2\cos\beta}, \tag{50}$$

where:

$$C_{24a} = \frac{\zeta \cos\alpha}{\omega K_c \left(\frac{1}{K_{s1}} + \frac{2\zeta \cos^2\alpha}{K_c} + \frac{\sin^2\alpha + \omega \sin\alpha \sin\beta}{K_{a1}} \right)}, \tag{51}$$

$$C_{24b} = \frac{\eta \cos\beta}{K_c \left(\frac{1}{K_{s2}} + \frac{2\eta \cos^2\beta}{K_c} + \frac{\omega \sin^2\beta + \sin\alpha \sin\beta}{\omega K_{a1}} \right)}, \tag{52}$$

$$C_{25a} = 1 + \frac{2\zeta \cos^2\beta}{K_c \left(\frac{1}{K_{s1}} + \frac{\sin^2\alpha + \omega \sin\alpha \sin\beta}{K_{a1}} \right)}, \tag{53}$$

$$C_{25b} = 1 + \frac{2\eta \cos^2\beta}{K_c \left(\frac{1}{K_{s2}} + \frac{\omega \sin^2\beta + \sin\alpha \sin\beta}{\omega K_{a1}} \right)}. \tag{54}$$

In this scenario, the behaviour is similar to that of a single-crossarm stayed column. Since T_1 is not an independent variable if $T_{2,i} \cos\beta > T_{1,i} \cos\alpha$, the limit of applicability of the two-parameter behaviour is depicted in Figure 8.

2.6. Determination of the zonal boundaries for Configuration 1

Using the same definitions outlined in Section 2.3, the minimum, linear optimal and maximum prestress can also be defined for Configuration 1, as presented in Figure 3. As for a single-crossarm stayed column, the lateral restraint in Configuration 1 is only provided by stay-group 1, thus giving:

$$T_{1,\min} = C_{11} P_{\mathrm{E}}, \quad T_{1,\mathrm{opt}} = C_{11} P_{\max}, \quad T_{1,\max} = \frac{P_{\max}}{2\cos\alpha}, \tag{55}$$

where:

$$P_{\max} = \frac{P_{T=0}}{C_{12}}, \quad C_{11} = \frac{\zeta \cos\alpha}{K_c \left(\frac{1}{K_{s1}} + \frac{2\zeta \cos^2\alpha}{K_c} + \frac{\sin^2\alpha}{K_{a1}} \right)}, \quad C_{12} = 1 + \frac{2\zeta \cos^2\alpha}{K_c \left(\frac{1}{K_{s1}} + \frac{\sin^2\alpha}{K_{a1}} \right)}. \tag{56}$$

Figure 9 shows the behaviour of Configuration 1, which is similar to that of a single-

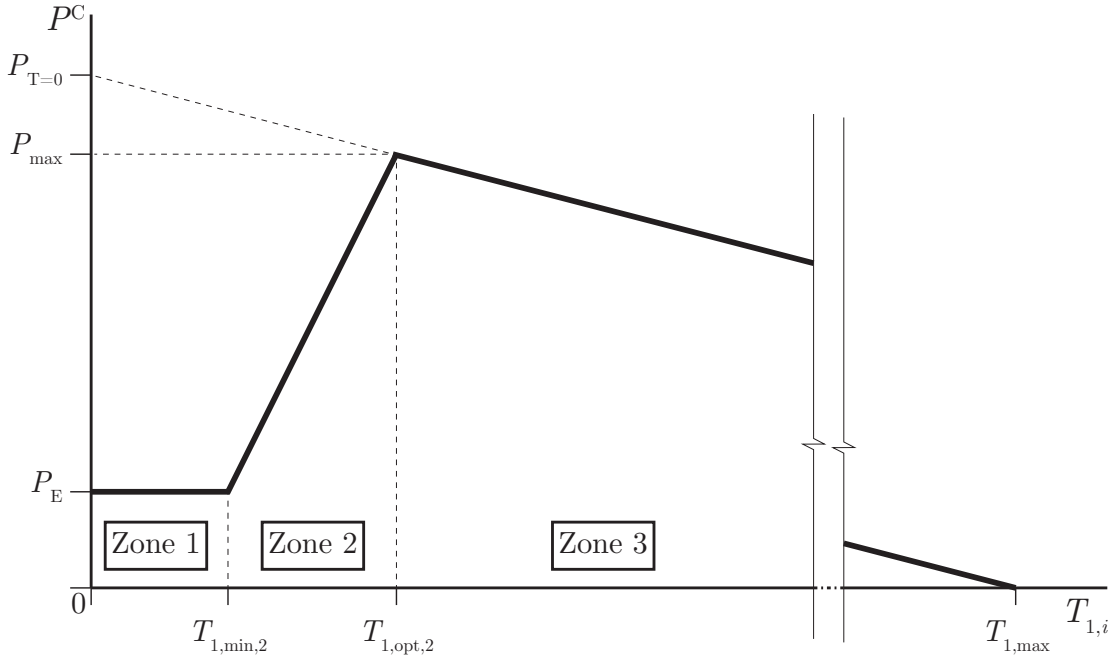

Figure 9: Critical buckling load P^{C} versus $T_{1,i}$ for Configuration 1.

crossarm stayed column [2]. The principal differences lie in the $\sin^2\alpha$ terms in C_{11} and C_{12}, which relate to the number of stays in each crossarm, as shown in Table 1.

Table 1: Comparison of C_{11} and C_{12} in Configuration 1 and the corresponding terms C_{11} and C_{22} for a single-crossarm stayed column where $K_a = E_a A_a/a$, A_a is the single-crossarm cross-sectional area and a is the length of the single crossarm.

Configuration 1	Single-crossarm stayed column [2]
$C_{11} = \frac{\cos\alpha}{2K_c\left(\frac{1}{K_{s1}}+\frac{\cos^2\alpha}{K_c}+\frac{\sin^2\alpha}{K_{a1}}\right)}$	$C_{11} = \frac{\cos\alpha}{2K_c\left(\frac{1}{K_{s1}}+\frac{\cos^2\alpha}{K_c}+\frac{2\sin^2\alpha}{K_a}\right)}$
$C_{12} = 1 + \frac{\cos^2\alpha}{K_c\left(\frac{1}{K_{s1}}+\frac{\sin^2\alpha}{K_{a1}}\right)}$	$C_{22} = 1 + \frac{\cos^2\alpha}{K_c\left(\frac{1}{K_{s1}}+\frac{2\sin^2\alpha}{K_a}\right)}$

3. Finite element modelling

A parametric finite element (FE) study is conducted within the commercial package Abaqus to validate the analytical results derived in Section 2 and assess the behaviour of stayed columns with additional stays at varying levels of initial pretension. The modelling parameters are based on those validated in previous work [22] and are depicted in Figure 10. The stayed column is modelled as a simply-supported member, with a pinned base and a

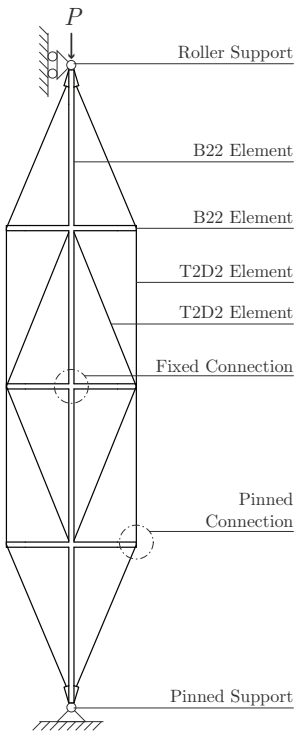

Figure 10: FE configuration showing element types with boundary and fixity conditions detailed.

roller support at the top, where a concentrated axial force is applied. The column and the crossarms are modelled using B22 Timoshenko beam elements and the stays are modelled with T2D2 truss elements with the 'no compression' option enabled to ensure the stays only resist tensile forces. These members are modelled with an elastic–perfectly plastic material assumed to allow for the influence of material nonlinearity on the structural behaviour. The crossarms and column are rigidly connected, while the stays are pinned to the column and the crossarms. Following an initial study, which compared the performance of the FE model described with that presented in previous research [22], it was determined that an element size of 25 mm in length for the column and the crossarms is sufficiently accurate, while a single element is used to model each stay to ensure a constant stress within those components.

A linear buckling analysis is initially conducted to obtain the distinct eigenvalues and eigenmodes. For each configuration considered, the buckling loads $P_{T=0}$ obtained are used to determine the maximum critical buckling load $P_{\max}$ and the linear optimal initial pretensioning force T_{opt}, as described in Section 2. Owing to the elastic deformations that occur after the application of the pretensioning force to the stays, the initial pretension force is increased accordingly such that the stress in the stays prior to the application of the load is at the desired level. The nonlinear Riks arc-length method [23] is used to validate the findings of the analytical relationships and to investigate the post-buckling behaviour for the three configurations. This method requires a perturbation to trigger the initial

instability in the FE model [24], which is introduced in the form of a vanishingly small initial imperfection, using a linear combination of buckling eigenmodes. This approach is consistent with the results of previous research [14]. It has been reported in the literature [11, 14, 15] that an imperfection amplitude of $L/10000$ is a sufficiently small perturbation to trigger the initial instability consistently while closely simulating the perfect behaviour of ideal stayed columns, and is therefore implemented herein. However, it should be stressed that a formal imperfection sensitivity analysis is not conducted in the current study; this is left for future work.

The parameters for the analyses are based on the values from an earlier study [19], as summarized in Table 2. The proportions selected ensure that local buckling within the main

Table 2: Model parameters for the FE simulations.

Parameter	Value
Main column: Young's Modulus, E	204.00 kN/mm^2
Main column: yield stress, f_{y}	355 N/mm^2
Main column: outside diameter, ϕ_o	57.2 mm
Main column: wall thickness, t	6.35 mm
Main column: length, L	6100 mm
Main column: normalized slenderness, $\bar{\lambda}$	4.47
Crossarm: Young's modulus, E_a	204.00 kN/mm^2
Crossarm: yield stress, f_{ya}	355 N/mm^2
Crossarm: outside diameter, ϕ_{ao}	57.2 mm
Crossarm: wall thickness, t_a	6.35 mm
Stays: Young's modulus, E_s	64.90 kN/mm^2
Stays: diameter, ϕ_s	6.4 mm
ω	1.0

column and the crossarm elements is not a concern. Local buckling within the individual elements of the stayed column would induce an extra dimension of complexity that would primarily reduce the buckling loads of the main column and possibly the crossarms. The possibility of local buckling could also induce the undesirable possibility of nonlinear mode interaction between local buckling modes and several global modes, which have been shown to be potentially catastrophically unstable in many systems [25, 26]. Such considerations are beyond the scope of the current study. The normalized slenderness of the main column $\bar{\lambda}$ is defined thus:

$$\bar{\lambda} = \sqrt{\frac{A_c f_{\mathrm{y}}}{P_{\mathrm{E}}}}, \tag{57}$$

and so for the example case, the theoretical critical buckling load of the main column element is approximately 5% of the main column *squash load*, defined as $A_c f_{\mathrm{y}}$. Hence, even including the system of crossarms and stays, buckling would occur with stresses that are well below the material elastic limit. The value of ω being set to unity implies that $L_1 = L/4$, as represented in Figures 4 and 7.

4. Results and discussion

The linear optimal pretensioning force T_{opt}, derived in Section 2, provides the maximum elastic critical buckling load. By definition, for a perfect system this is the load at which the pretension in all the stays instantaneously vanishes at critical buckling. At this instance, the stays no longer provide any lateral restraint at the location of the crossarms causing buckling to occur. However, in real stayed columns and indeed in the FE analyses conducted, geometric imperfections cause the system to deflect laterally from the onset of loading. Therefore, when the stays on the concave side of the main column element instantaneously go slack, the stays on the convex side of the column are instantly reactivated resulting in an increased load-carrying capacity. The buckling load, as defined in the analytical derivation of T_{opt}, is not easily detected in a nonlinear FE analysis. Different methodologies for the assessment of the behaviour were explored to assess the validity of the derived value of T_{opt}. A qualitative analysis of the post-buckling curves in relation to the findings in [8] would seem to be the most consistent and effective approach.

4.1. Validation of linear optimal prestress expressions

Validation of the linear optimal prestress expressions for Configurations 2 and 3 is carried out for the case of $2a/L = 0.15$, where Mode 1, the classical half-sine wave eigenmode for a simply-supported column under pure compression as depicted in Figure 11, is critical.

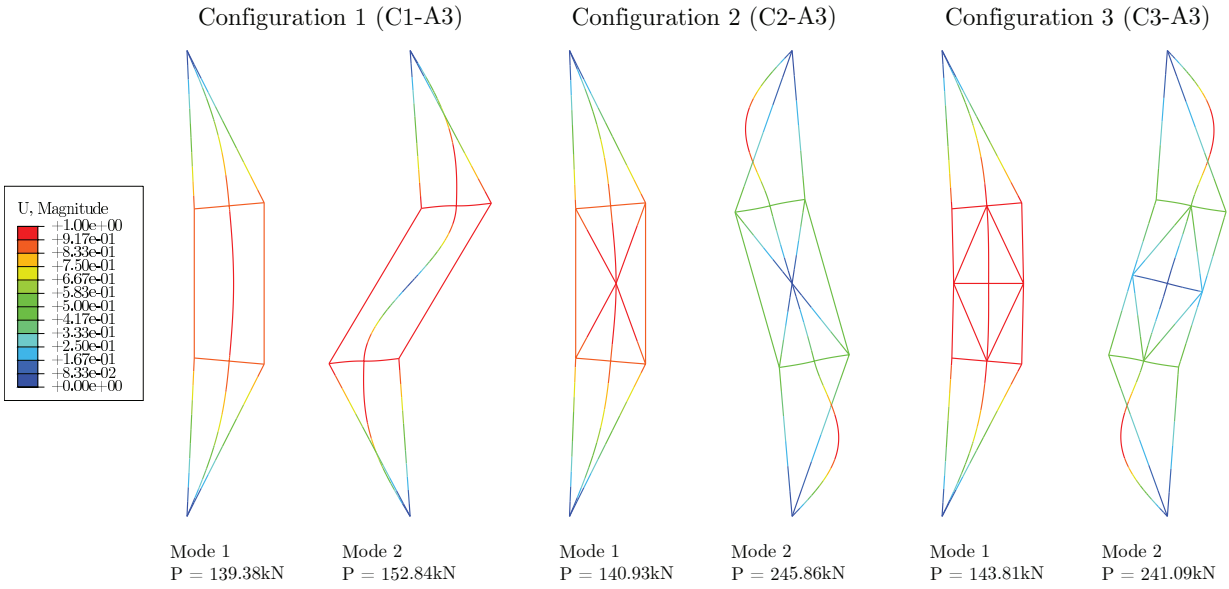

Figure 11: First two eigenmodes and corresponding eigenvalues from the linear buckling analysis of Configurations 1, 2 and 3 respectively. Column deflections have been deliberately exaggerated to depict the buckling modes clearly.

As discussed in Section 3, a perturbation scaling the first eigenmode by $L/10000$ is used to trigger the initial instability in the FE Model. The stays are modelled in three groups, where all stays in each group are assigned the same initial pretension, with T_1 and T_2 as

the independent variables in the parametric analysis. The properties of the stays are kept constant to reduce the number of variables in the study.

Discrete multiples of $T_{1,\text{opt},0}$ and $T_{2,\text{opt},0}$, together with all their permutations, are studied by FE to determine the validity of the analytical solutions along with the influence of the initial pretension forces on the behaviour of the stayed column. The analytical solutions for the minimum and linear optimal initial pretensioning forces are presented in Tables 3 and 4. Previous research [2, 4, 14] has shown that in single crossarm stayed

Table 3: T_{min} and T_{opt} for Configuration 3 (C3).

Ref	$2a/L$	$P_{T=0}$ Mode 1 [kN]	$P_{T=0}$ Mode 2 [kN]	Critical Mode	P_{max} [kN]	$T_{1,\text{min},0}$ [kN]	$T_{1,\text{opt},0}$ [kN]	$T_{2,\text{min},0}$ [kN]	$T_{2,\text{opt},0}$ [kN]
C3-A1	0.05	42.58	115.85	1	40.95	0.176	0.401	0.176	0.40
C3-A2	0.10	104.29	200.69	1	100.47	0.172	0.956	0.171	0.96
C3-A3	0.15	194.14	302.74	1	187.49	0.164	1.705	0.164	1.70
C3-A4	0.20	300.54	399.43	1	291.14	0.154	2.491	0.154	2.49
C3-A5	0.25	398.12	449.45	1	386.96	0.143	3.076	0.143	3.07
C3-A6	0.30	445.70	459.40	1	434.66	0.132	3.180	0.132	3.18

Table 4: T_{min} and T_{opt} for Configuration 2 (C2).

Ref	$2a/L$	$P_{T=0}$ Mode 1 [kN]	$P_{T=0}$ Mode 2 [kN]	Critical Mode	P_{max} [kN]	$T_{1,\text{min},0}$ [kN]	$T_{1,\text{opt},0}$ [kN]	$T_{2,\text{min},0}$ [kN]	$T_{2,\text{opt},0}$ [kN]
C2-A1	0.05	40.66	104.55	1	39.87	0.18	0.39	0.18	0.40
C2-A2	0.10	92.68	195.39	1	90.95	0.17	0.87	0.18	0.88
C2-A3	0.15	163.97	316.43	1	161.11	0.16	1.47	0.17	1.49
C2-A4	0.20	250.31	424.47	1	246.33	0.15	2.11	0.16	2.14
C2-A5	0.25	347.28	441.25	1	342.34	0.14	2.72	0.15	2.76
C2-A6	0.30	440.95	431.33	2	425.92	0.13	3.12	0.53	3.16

columns, an increase in $2a/L$ results in an increase in the lateral restoring force component that restrains the column against the buckling displacement. Since Mode 1 has a maximum lateral deflection at midspan, its corresponding buckling load is more affected by an increase in $2a/L$ than the buckling load for Mode 2, which, in contrast, has zero midspan lateral deflection. Subsequently, for higher values of $2a/L$, Mode 2 becomes critical. The same observations hold true for Configurations 2 and 3, as is noted in Tables 3 and 4.

Figure 12 shows the equilibrium paths for the case C3-A3 when $T_2/T_{2,\text{opt},0} = 0.0$ and 2.0 in (a) and (b) respectively for varying levels of $T_1/T_{1,\text{opt},0}$. For the case where T_2 is zero, $T_{1,\text{opt},0}$ as determined by the procedure in Section 2.4, is 1.705 kN. The figure shows that at precisely this initial pretension force the behaviour shifts from Zone 2 to Zone 3. For the case where $T_2/T_{2,\text{opt},0} = 2.0$, the analytical model predicts that for any initial pretension

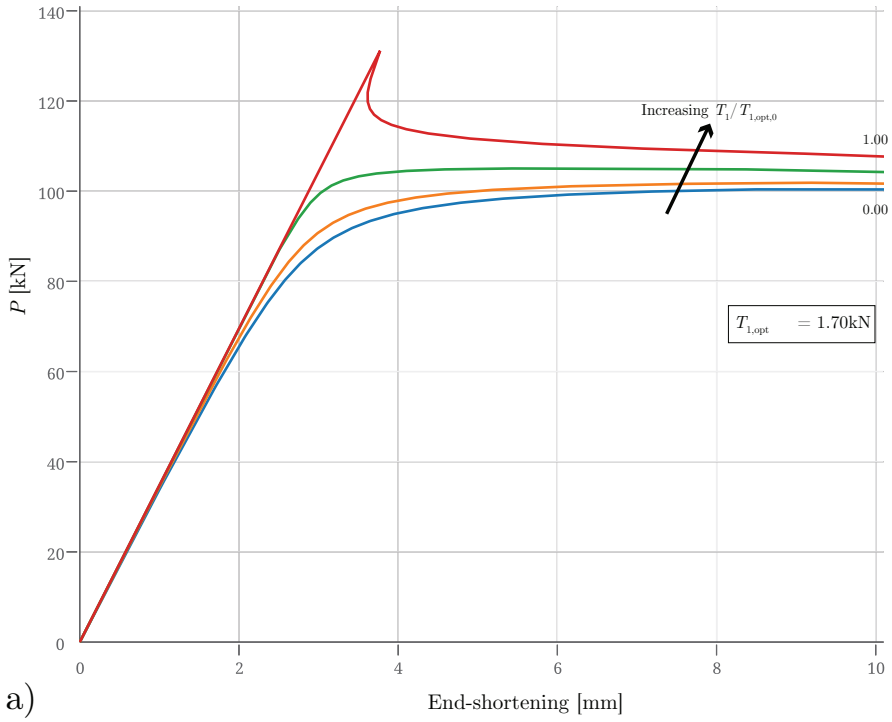

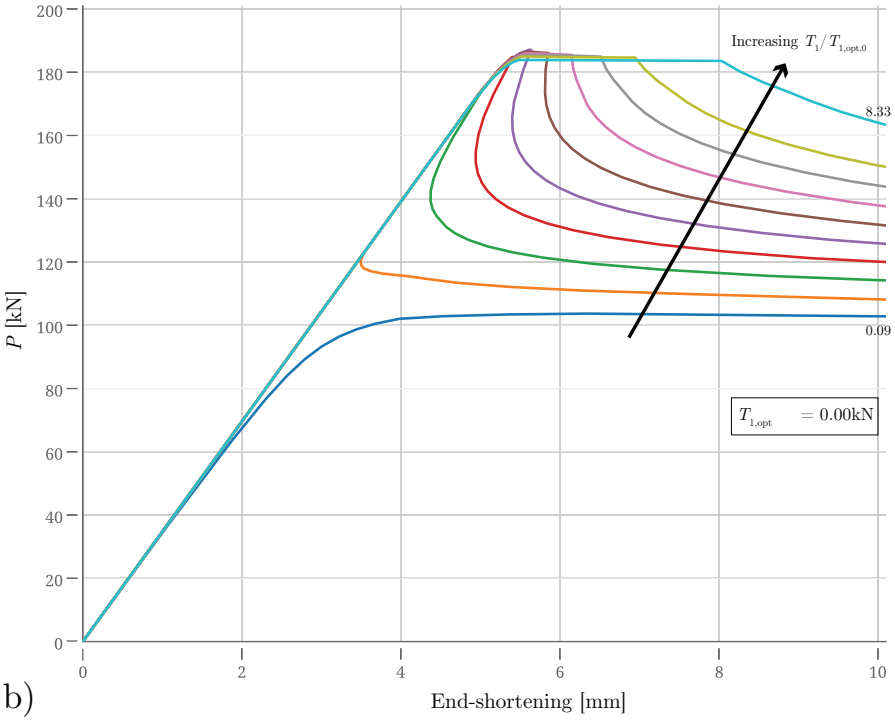

Figure 12: Load versus end-shortening curves for case C3-A3, when $T_2/T_{2,\mathrm{opt},0}$, is (a) 0.0 and (b) 2.0. Numerical values of $T_1/T_{1,\mathrm{opt},0}$ are labelled for relevant curves.

applied for T_1, the behaviour should be within Zone 3. Figure 12(b) suggests that when $T_2/T_{2,\text{opt},0} > 1.0$, the initial pretension force specified for stay-group 1 must be greater than $T_{1,\text{opt},0}$ to ensure that the behaviour of the stayed column is within Zone 3.

Figure 13(a) shows the equilibrium paths for the case C2-A3 with varying levels of $T_1/T_{1,\text{opt},0}$ when $T_2/T_{2,\text{opt},0} = 0.5$. Using the procedure described in Section 2.4, for this level of initial pretension in stay-group 2, $T_{1,\text{opt}}$ is found to be 1.465 kN and therefore $T_{1,\text{opt}}/T_{1,\text{opt},0} = 1.0$. When $T_1/T_{1,\text{opt},0} < 1$, Figure 13(a) depicts a stable post-buckling response which is indicative of the behaviour in Zone 1 and a portion of Zone 2, as described in [8]. Moreover, when $T_1/T_{1,\text{opt},0} \geqslant 1$, the sharp drop in post-buckling resistance is indicative of the early stages of Zone 3, suggesting the shift in the behaviour has been predicted accurately. Note also that as T_1 is increased beyond $T_{1,\text{opt},0}$, there is a significant plateau before any unloading, implying unstable post-buckling behaviour, is observed.

Similarly, Figure 13(b) shows the results from the analyses when $T_2/T_{2,\text{opt},0} = 2.0$. The analytical formulation suggests that for this level of initial pretension in stay-group 2, $T_{1,\text{opt}}$ is zero and thus the behaviour of the system should be directly within Zone 3 regardless of T_1. However, when $T_1/T_{1,\text{opt},0} < T_2/T_{2,\text{opt},0}$, the behaviour is not indicative of Zone 3, as shown by the stable post-buckling equilibrium paths.

For combinations of T_1 and T_2, where $T_2 \cos\beta > T_1 \cos\alpha$, pre-buckling deformation states, which are different to those assumed in Figure 7, are observed and are thus outside the range of validity of the derivations in Section 2.5, as discussed in Section 2.1. This highlights the reason that in actual stayed columns $T_{1,\text{opt}}$ is not zero when $T_2/T_{2,\text{opt},0} > 1$. It is demonstrated that for the solution to be within Zone 3 when $\omega = 1.0$ and $T_2/T_{2,\text{opt},0} > 1$, the initial pretension force specified for stay-group 1 must satisfy the condition: $T_1/T_{1,\text{opt},0} \geqslant T_2/T_{2,\text{opt},0}$. This behaviour is consistently noted for other levels of $T_2/T_{2,\text{opt},0}$ from the current study.

The difference between the analytical and the FE model results is attributed to the latter considering higher order kinematic relationships for the deformation than those assumed in the analytical formulation. In both scenarios, a more detailed analysis of the stays that remain active in the post-buckling range, thereby determining whether the buckled stayed column is stable or otherwise, has not been explored in the current study and has been left for the future.

4.2. Influence of multiple stays in Configuration 3

Having demonstrated the validity of the derived linear optimal prestress, the effect of the initial pretension force for Configuration 3 is analysed by means of a parametric FE study that involves determining the ultimate capacity of the stayed columns with a simultaneous variation in $T_1/T_{1,\text{opt},0}$ and $T_2/T_{2,\text{opt},0}$. The results are depicted in Figure 14 which shows a contour plot grouping bands of P_{ult}, as determined from the parametric study. In this configuration, both stay-groups 1 and 2 contribute to the behaviour of the system. Thus, the absence of either $T_1/T_{1,\text{opt},0}$ or $T_2/T_{2,\text{opt},0}$ has a detrimental effect on the load-carrying capacity of the stayed column. This is confirmed in Figure 14 by the contour not reaching the highest band at 180 kN if either T_1 or T_2 are zero. It is also noted that Figure 14 is comparable to the analytical contour plot presented in Figure 6(a).

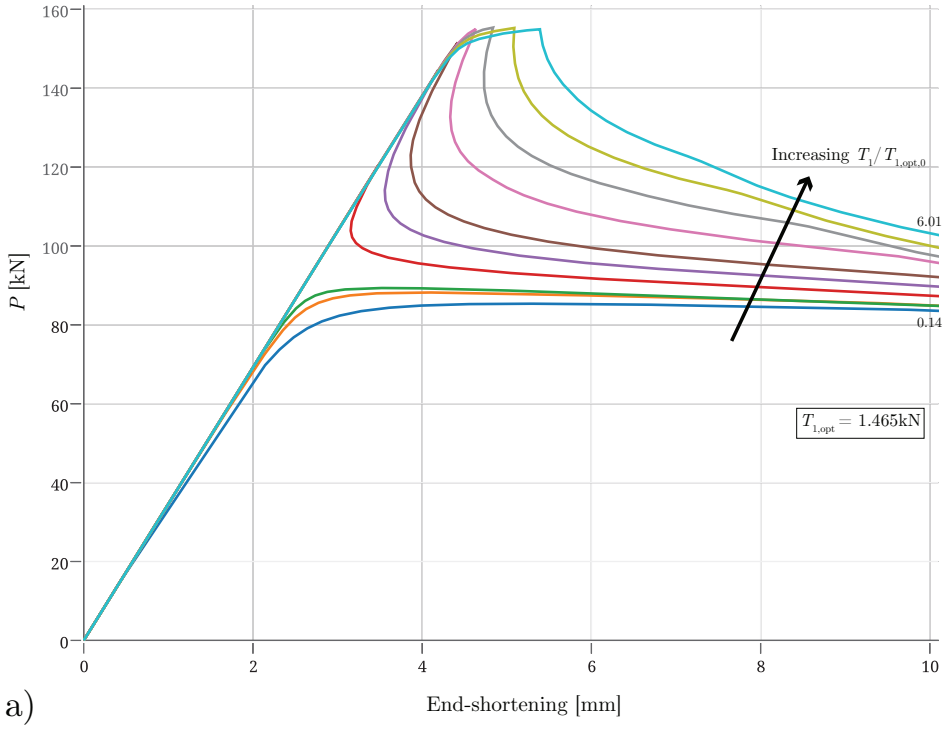

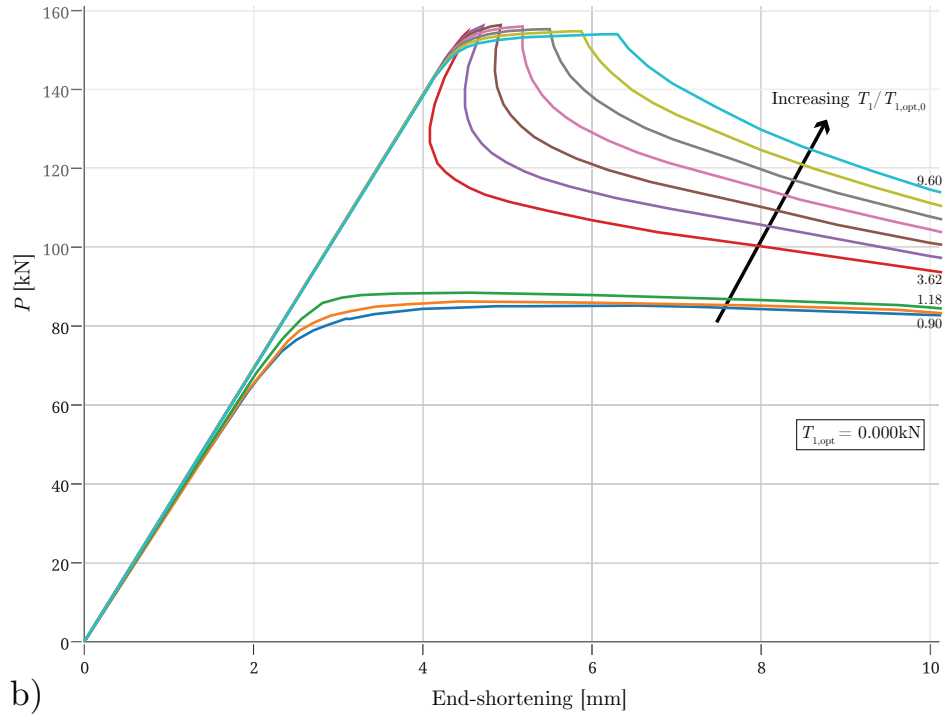

Figure 13: Load versus end-shortening curves for case C2-A3, when $T_2/T_{2,\mathrm{opt},0}$ is (a) 0.5 and (b) 2.0. Numerical values of $T_1/T_{1,\mathrm{opt},0}$ are labelled for relevant curves.

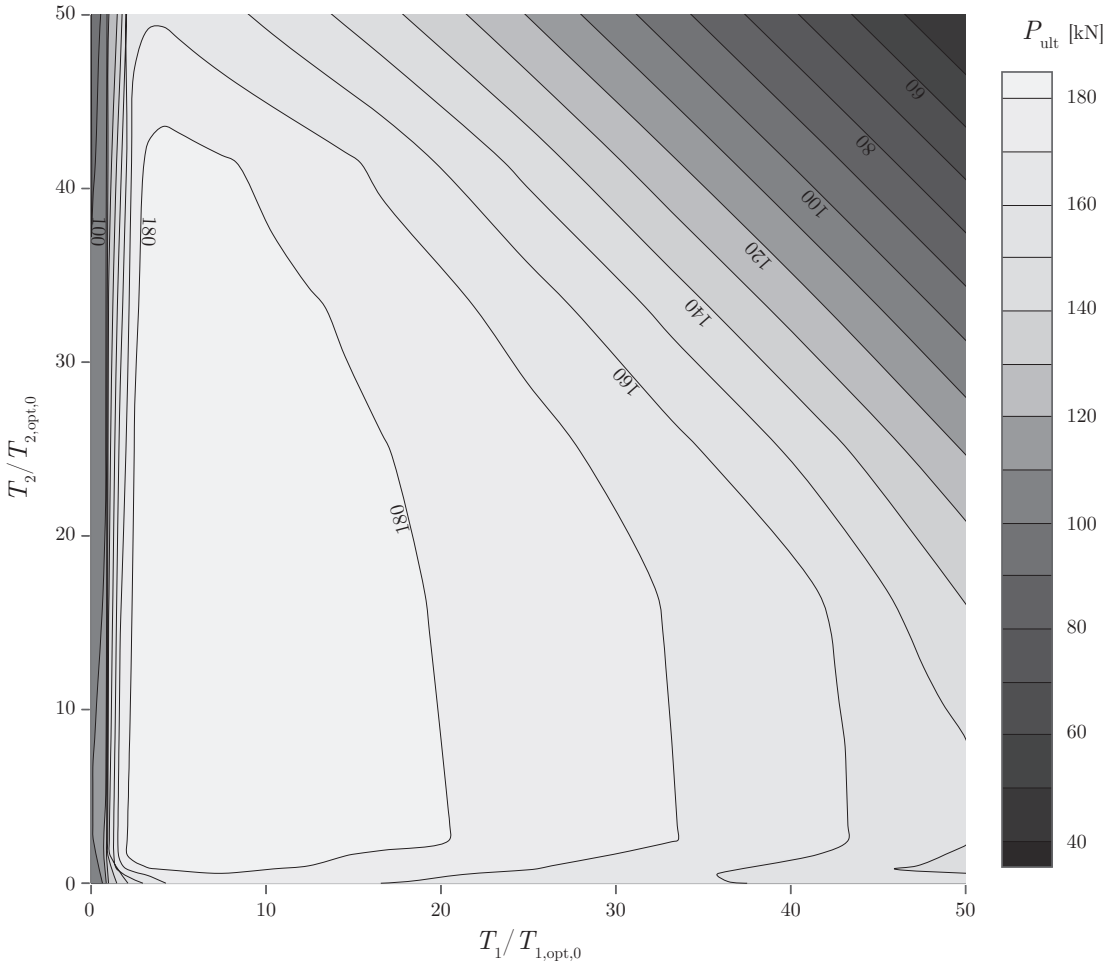

Figure 14: Contour plot showing variation of the load-carrying capacity for Configuration 3 while varying $T_1/T_{1,\text{opt},0}$ and $T_2/T_{2,\text{opt},0}$.

For $\omega = 1.0$, the analytical and FE solutions both show that for $T_1/T_{1,\text{opt},0}$ and $T_2/T_{2,\text{opt},0}$ being well above unity, there is an equally detrimental effect to the load-carrying capacity of the stayed column.

The load-carrying capacity obtained for $T_1/T_{1,\text{opt},0}$ at various levels of $T_2/T_{2,\text{opt},0}$ is compared with the analytical predictions for P^{C} in Figures 15 and 16. The trends observed

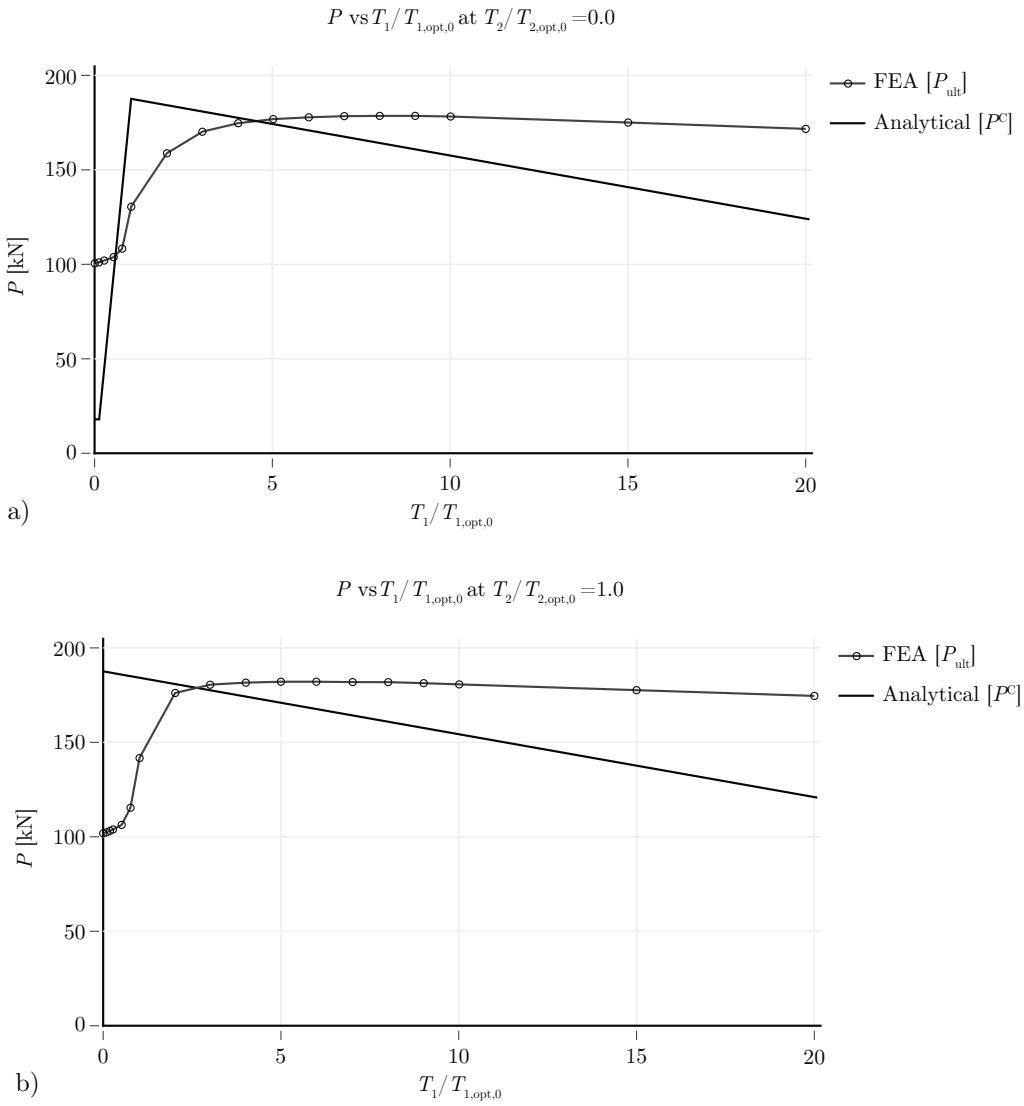

Figure 15: Maximum load-carrying capacity versus $T_1/T_{1,\text{opt},0}$ for two different cases where $T_2/T_{2,\text{opt},0}$ is (a) 0.0 and (b) 1.0 in comparison with the analytical solutions for Configuration 3.

are similar to those of a single-crossarm stayed column, such as those reported in [22]. The difference in the analytical graphs lies where $T_2/T_{2,\text{opt},0} \geqslant 1.0$ in Figures 15(b) and 16, which lacks the initial linearly increasing portion. This is attributed to the analytical solution for $T_2/T_{2,\text{opt},0}$ being already defined within Zone 3 regardless of the value of $T_1/T_{1,\text{opt},0}$. As mentioned earlier, the discrepancies between the analytical and FE solutions are primarily

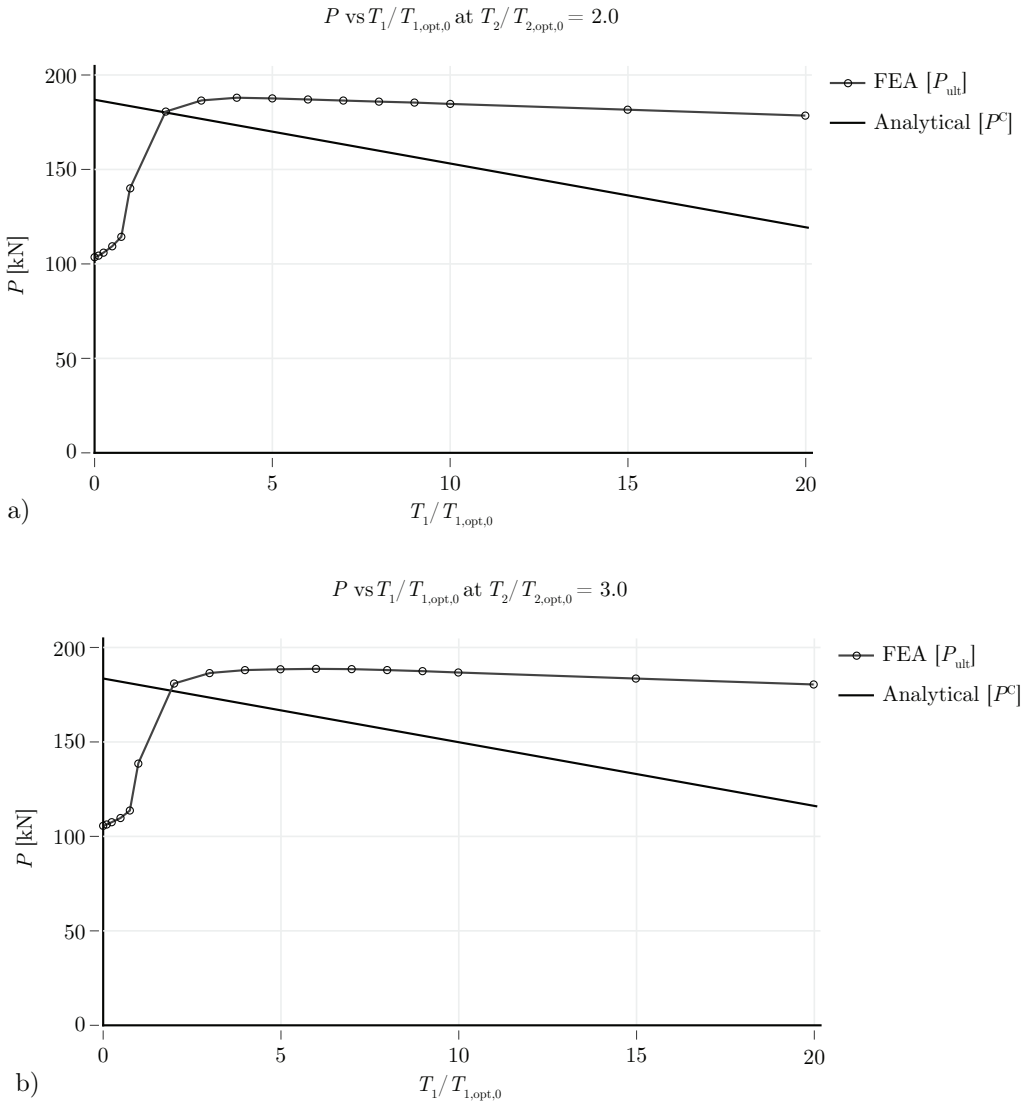

Figure 16: Maximum load-carrying capacity versus $T_1/T_{1,\mathrm{opt},0}$ for two different cases where $T_2/T_{2,\mathrm{opt},0}$ is (a) 2.0 and (b) 3.0 in comparison with the analytical solutions for Configuration 3.

due to the different respective definitions of the predicted failure load. The analytical model is based on linear theory and therefore the linear nature of the curves is purely a consequence of the assumption of perfect geometry. However, the presence of imperfections, or even a vanishingly small perturbation, introduces nonlinearities to the behaviour as soon as external loading is introduced, as observed in the results from the FE model. Corresponding findings are also noted in previous studies [4, 10].

4.3. Influence of multiple stays in Configuration 2

Similarly, the effect of the initial pretension force for Configuration 2 is analysed by means of a parametric FE study, which determines the ultimate capacity of the stayed columns with a simultaneous increase in $T_1/T_{1,\mathrm{opt},0}$ and $T_2/T_{2,\mathrm{opt},0}$. The results are depicted in Figure 17. The 'ripples' noted in the contour plots in Figure 17 (and earlier in Figure

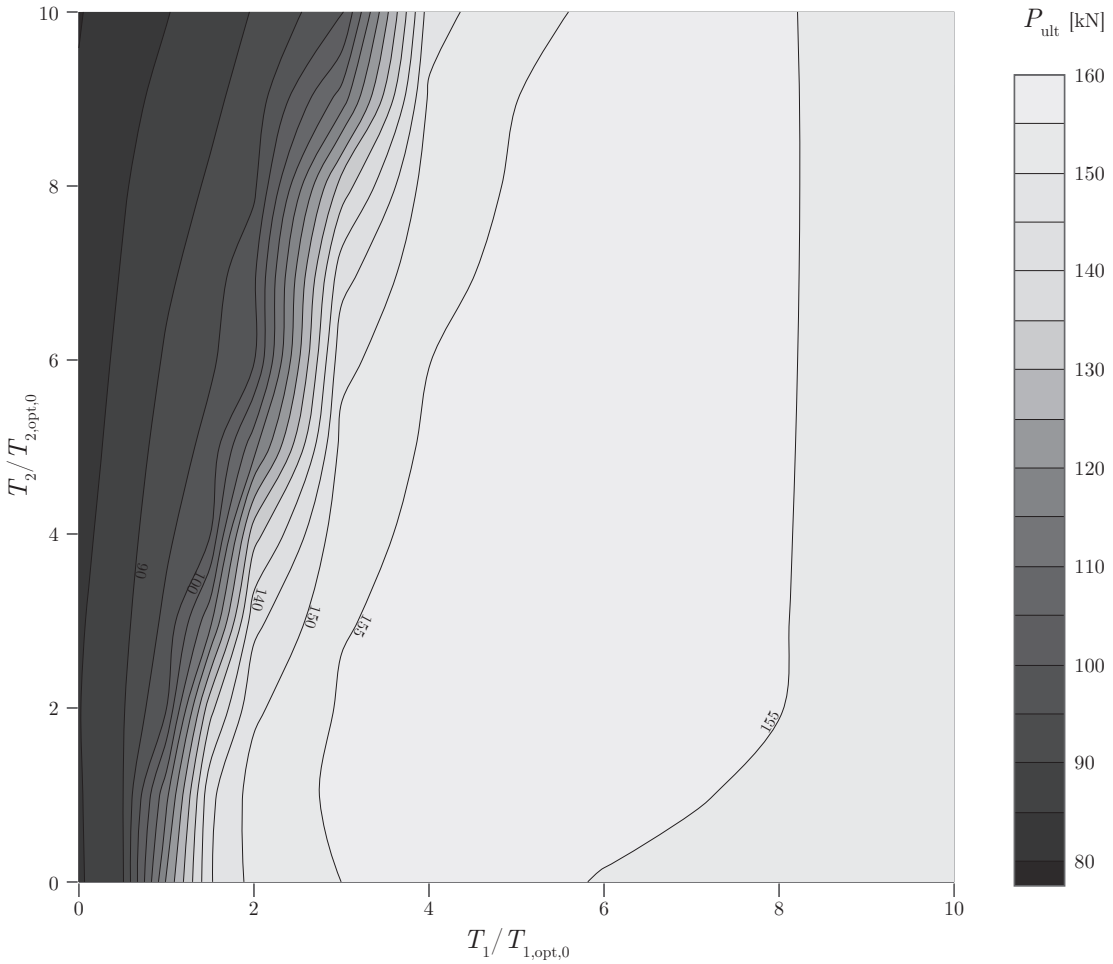

Figure 17: Contour plot showing variation of the load-carrying capacity for Configuration 2 while varying $T_1/T_{1,\mathrm{opt},0}$ and $T_2/T_{2,\mathrm{opt},0}$.

14) are due to the number of permutations of T_1 and T_2 included, which were limited to balance the resolution of the solutions with the computational effort required.

Contrary to the behaviour noted in Configuration 3, the effects of the initial pretension in stay-group 1 and stay-group 2 are not equally effective in Configuration 2. The contour plot in Figure 17 clearly illustrates this relationship, where an increase in $T_1/T_{1,\text{opt},0}$ has a more direct effect on the ultimate load achieved, when compared to a similar relative increase in $T_2/T_{2,\text{opt},0}$. This is illustrated by the direction of the contours being essentially perpendicular to the T_1 axis in Figure 17. In the parametric study for Configuration 2, the limiting condition described in Section 2.5, where $T_1 \cos\alpha > T_2 \cos\beta$ and therefore stay-group 1 provides a greater lateral force when compared to stay-group 2, is not always upheld. These observations are noted in Figure 17 where, for an increase in $T_2/T_{2,\text{opt},0}$, a larger initial pretension force in stay-group 1 is required to achieve the same load-carrying capacity. This behaviour is attributed to the fact that some of the stay forces introduce bending in the crossarms, thereby reducing their effectiveness as lateral restraints and hence legitimizing the final assumption made in Section 2.1.

4.4. Real optimum initial pretension

Previous work [6, 7] discussed the 'real optimum initial pretension' in stayed columns in single and triple crossarm systems respectively. It was noted in both works that the maximum load-carrying capacity of a member is not a mutually comparable indicator of effectiveness for different configurations. Terms were proposed identifying the column and the stay efficiencies to allow for the selection of an appropriate structural configuration and an optimal level of initial prestress. The current study has not gone to the same depth, but defines the 'real optimum initial pretension' presently as the lowest possible initial pretension to achieve the highest load-carrying capacity for the parameters considered. For the case C2-A3, this is noted at $T_1/T_{1,\text{opt},0} \geqslant 3$ and $T_2/T_{2,\text{opt},0} \geqslant 1$, where the load-carrying capacity is approximately 160 kN. In the equivalent case for Configuration 1 (with only one stay-group), the maximum load-carrying capacity occurs when $T_1/T_{1,\text{opt},0} \approx 3$, where the ultimate load is found to be 100 kN. A simple comparison between the two demonstrates an increase in capacity of approximately 60%, which shows the effectiveness of the additional stay system.

Meanwhile, for Configuration 3, the real optimum initial pretension, as defined, is observed to occur at values of $T_1/T_{1,\text{opt},0} \approx 3$ and $T_2/T_{2,\text{opt},0} \approx 2$, with an ultimate resistance load approximately equal to 190 kN. This shows an increase in load-carrying capacity of approximately 90% when compared to Configuration 1, which once again represents a substantial enhancement in axial strength. These values are taken from a single comparison; further research would therefore be required where the relative effects of different parameters are compared, such as the length and the location of crossarms, over a larger parametric space to determine the representative change in load-carrying capacity for the different configurations. It is highlighted that the nature of the geometry in Configuration 3 is more effective in resisting flexural buckling than that of Configuration 2. This is specifically the case when discussing stay-group 2, on account of the additional crossarm providing a greater resistance to buckling at mid-height of the main column element, where the lateral deflection tends to be the largest.

5. Concluding remarks

The current work has investigated the behaviour of prestressed stayed columns with multiple crossarms and additional stays. A primary outcome is the analytical determination of the three zones of behaviour, defining the linear buckling response of the system but now in three-dimensional parametric space, owing to the additional stay group, rather than in two-dimensional parametric space as before [2]. In each of the considered configurations, equilibrium of the internal forces was established after the application of the initial pretension and, in the pre-buckling deformation state, after the application of an external load.

The minimum ($T_{\min}$), linear optimal (T_{opt}) and maximum ($T_{\max}$) initial pretension forces obtained theoretically were validated using FE analysis, showing good correlation in all configurations, with the exception of certain specified permutations of the forces in the individual stay groups in Configurations 2 and 3 as presented. Previous research [6] has identified that T_{opt} is not the initial pretension that provides the truly optimal structural response due to the effects of nonlinearity. The current study has evaluated the corresponding quantities for different stay-groups based on the initial pretension that provides the highest load-carrying capacity for the least initial pretension. This identifies the conditions for Configurations 2 and 3 where the system is most effective in increasing the load-carrying capacity of the stayed columns. An analysis of the maximum load-carrying capacity in the post-buckling range for Configurations 2 and 3 shows that there is a significant increase in load-carrying capacity when compared to Configuration 1 where no extra stay-groups are provided. It is the intention to extend the work to consider the implications of the current findings for the post-buckling stability and the resulting sensitivity to geometric imperfections. Moreover, investigation of the effects of residual stresses within the main column and cross-sectional slendernesses of the main column and the crossarm elements will be conducted. This would ensure that designers are able to use this innovative structural system both safely and efficiently.

References

[1] E. Belenya, Prestressed load-bearing metal structures, Moscow: Mir Publishers, 1977.

[2] H. H. Hafez, M. C. Temple, J. S. Ellis, Pretensioning of single-crossarm stayed columns, ASCE J. Struct. Div. 105 (2) (1979) 359–375.

[3] E. A. Smith, Discussion of "Pretensioning of single-crossarm stayed columns", by Hafez, HH, Temple MC, Ellis JS, ASCE J. Struct. Div. 105 (11) (1979) 2482–2485.

[4] M. C. Temple, M. V. Prakash, J. S. Ellis, Failure criteria for stayed columns, ASCE J. Struct. Div. 110 (1984) 2677–2689.

[5] S. L. Chan, G. Shu, Z. Lü, Stability analysis and parametric study of pre-stressed stayed columns, Eng. Struct. 24 (1) (2002) 115–124.

[6] D. Saito, M. A. Wadee, Optimal prestressing and configuration of stayed columns, Proc. Instn. Civil Eng. – Struct. Build. 163 (5) (2010) 343–355.

[7] J. Yu, M. A. Wadee, Optimal prestressing of triple-bay prestressed stayed columns, Structures 12 (2017) 132–144.

[8] D. Saito, M. A. Wadee, Post-buckling behaviour of prestressed steel stayed columns, Eng. Struct. 30 (5) (2008) 1224–1239.

[9] E. A. Smith, Behavior of columns with pretensioned stays, ASCE J. Struct. Eng. 111 (5) (1985) 961–972.

[10] M. A. Wadee, L. Gardner, A. I. Osofero, Design of prestressed stayed columns, J. Constr. Steel Res. 80 (2013) 287–298.

[11] D. Saito, M. A. Wadee, Buckling behaviour of prestressed steel stayed columns with imperfections and stress limitation, Eng. Struct. 31 (1) (2009) 1–15.

[12] P. Li, M. A. Wadee, J. Yu, M. Wu, Stability of prestressed stayed steel columns with a three branch crossarm system, J. Constr. Steel Res. 122 (2016) 274–291.

[13] R. Pichal, J. Machacek, Buckling and post-buckling of prestressed stainless steel stayed columns, Procedia Eng. 172 (2017) 875–882.

[14] D. Saito, M. A. Wadee, Numerical studies of interactive buckling in prestressed steel stayed columns, Eng. Struct. 31 (2) (2009) 432–443.

[15] J. Yu, M. A. Wadee, Mode interaction in triple-bay prestressed stayed columns, Int. J. Non-Linear Mech. 88 (2017) 47–66.

[16] R. R. de Araujo, S. A. L. de Andrade, P. C. G. d. S. Vellasco, J. G. S. da Silva, L. R. O. de Lima, Experimental and numerical assessment of stayed steel columns, J. Constr. Steel Res. 64 (9) (2008) 1020–1029.

[17] A. I. Osofero, M. A. Wadee, L. Gardner, Experimental study of critical and post-buckling behaviour of prestressed stayed columns, J. Constr. Steel Res. 79 (2012) 226–241.

[18] M. Serra, A. Shahbazian, L. Simões da Silva, L. Marques, C. Rebelo, P. C. G. d. S. Vellasco, A full scale experimental study of prestressed stayed columns, Eng. Struct. 100 (2015) 490–510.

[19] M. C. Temple, Buckling of stayed columns, ASCE J. Struct. Div. 103 (4) (1977) 839–851.

[20] J. Van Steirteghem, W. P. De Wilde, P. Samyn, B. P. Verbeeck, F. Wattel, Optimum design of stayed columns with split-up cross arm, Adv. Eng. Softw. 36 (9) (2005) 614–625.

[21] J. P. Martins, A. Shahbazian, L. Simões da Silva, C. Rebelo, R. Simões, Structural behaviour of prestressed stayed columns with single and double cross-arms using normal and high strength steel, Arch. Civil Mech. Eng. 16 (4) (2016) 618–633.

[22] A. I. Osofero, M. A. Wadee, L. Gardner, Numerical studies on the buckling resistance of prestressed stayed columns, Adv. Struct. Eng. 16 (3) (2013) 487–498.

[23] E. Riks, An incremental approach to the solution of snapping and buckling problems, Int. J. Solids Struct. 15 (7) (1979) 529–551.

[24] T. Belytschko, W. K. Liu, B. Moran, Nonlinear finite elements for continua and structures, Wiley, Chichester, 2000.

[25] B. Budiansky (Ed.), Buckling of structures, Springer, Berlin, 1976, IUTAM symposium.

[26] J. M. T. Thompson, G. W. Hunt, Elastic instability phenomena, Wiley, Chichester, 1984.